HAL
open science

Contribution of mixing to the upward transport across the TTL

P. Konopka, G. Günther, R. Müller, F. H. S. dos Santos, C. Schiller, F. Ravegnani, A. Ulanovsky, H. Schlager, C. M. Volk, S. Viciani, et al.

To cite this version:

P. Konopka, G. Günther, R. Müller, F. H. S. dos Santos, C. Schiller, et al.. Contribution of mixing to the upward transport across the TTL. Atmospheric Chemistry and Physics Discussions, 2006, 6 (6), pp.12217-12266. hal-00302320

HAL Id: hal-00302320

https://hal.science/hal-00302320v1

Submitted on 18 Jun 2008

HAL is a multi-disciplinary open access archive for the deposit and dissemination of scientific research documents, whether they are published or not. The documents may come from teaching and research institutions in France or abroad, or from public or private research centers.

L'archive ouverte pluridisciplinaire **HAL**, est destinée au dépôt et à la diffusion de documents scientifiques de niveau recherche, publiés ou non, émanant des établissements d'enseignement et de recherche français ou étrangers, des laboratoires publics ou privés.

Atmos. Chem. Phys. Discuss., 6, 12217–12266, 2006
www.atmos-chem-phys-discuss.net/6/12217/2006/
© Author(s) 2006. This work is licensed
under a Creative Commons License.

Atmospheric Chemistry and Physics Discussions

Contribution of mixing to the upward transport across the TTL

P. Konopka[1], G. Günther[1], R. Müller[1], F. H. S. dos Santos[1], C. Schiller[1], F. Ravegnani[2], A. Ulanovsky[3], H. Schlager[4], C. M. Volk[5], S. Viciani[6], L. Pan[7], D.-S. McKenna[7], and M. Riese[1]

[1]Forschungszentrum Jülich (ICG-I: Stratosphere), Germany
[2]CNR-ISAC, Bologna, Italy
[3]CAO, Dolgoprudny, Russia
[4]Institut für Physik der Atmosphäre, DLR Oberpfaffenhofen, Germany
[5]Institut für Meteorologie und Geophysik, Universität Frankfurt, Germany
[6]INOA, Firenze, Italy
[7]National Center for Atmospheric Research, Boulder, CO, USA

Received: 25 October 2006 – Accepted: 22 November 2006 – Published: 28 November 2006

Correspondence to: P. Konopka (p.konopka@fz-juelich.de)

Abstract

During the second part of the TROCCINOX campaign that took place in Brazil in early 2005, chemical species were measured on-board of the high altitude research aircraft Geophysica (ozone, water vapor, NO, NO_y, CH_4 and CO) in the altitude range up to 20 km (or up to 450 K potential temperature), i.e. spanning the TTL region roughly extending between 350 and 420 K.

Analysis of transport across TTL is performed using a new version of the Chemical Lagrangian Model of the Stratosphere (CLaMS). In this new version, the stratospheric model has been extended to the earth surface. Above the tropopause, the isentropic and cross-isentropic advection in CLaMS is driven by ECMWF winds and heating/cooling rates derived from a radiation calculation. Below the tropopause the model smoothly transforms from the isentropic to hybrid-pressure coordinate and, in this way, takes into account the effect of large-scale convective transport as implemented in the ECMWF vertical wind. As with other CLaMS simulations, the irreversible transport, i.e. mixing, is controlled by the local horizontal strain and vertical shear rates.

Stratospheric and tropospheric signatures in the TTL can be seen both in the observation and in the model. The composition of air above ≈350 K is mainly controlled by mixing on a time scale of weeks or even months. Based on CLaMS transport studies where mixing can be completely switched off, we deduce that vertical mixing, mainly driven by the vertical shear in the outflow regions of the large-scale convection and in the vicinity of the subtropical jets, is necessary to understand the upward transport of the tropospheric air from the main convective outflow around 350 K up to the tropical tropopause around 380 K. This mechanism is most effective if the outflow of the mesoscale convective systems interacts with the subtropical jets.

1 Introduction

The composition of the air entering the stratosphere is mainly determined by the transport processes within the tropical tropopause layer (TTL) (Atticks and Robinson, 1983) coupling the Hadley circulation in the tropical troposphere with the much slower, Brewer-Dobson circulation in the stratosphere. Whereas the first one is dominated by convective processes, the latter one is mainly driven by radiation and extratropical wave drag (Holton et al., 1995).

The lowest boundary of the TTL around θ=350 K isentropic surface (see Fig. 1) can be defined as the level of the main convective outflow (Folkins and Martin, 2005). The upper TTL limit is expected to be above the cold point tropopause at around 380 K but below ≈420 K marking the highest level of the observed deepest convection events (Kelly et al., 1993; Sherwood and Dessler, 2001).

Laterally, the TTL is confined by the subtropical jets (STJ) which vary seasonally both their intensity and meridional position with a strong, equatorwards shifted jet in the winter hemisphere (WH) and a weak, meandering, poleward shifted STJ in the summer hemisphere (SH). Following the concept of effective diffusivity, Haynes and Shuckburgh (2000) showed that a strong STJ forms an effective transport barrier for the meridional, isentropic transport between the TTL and mid latitudes with highest permeability during monsoon circulations, mainly in the NH, when a strong upper-level anticyclone over south-east Asia disrupts the zonal symmetry of the STJ. Furthermore, Haynes and Shuckburgh (2000) concluded that STJ in the SH is generally a stronger transport barrier than STJ in the NH during the same season.

Because deep convection events transporting air directly into the stratosphere seem to be too rare to supply the Brewer-Dobson circulation with sufficient mass (Gettelman et al., 2002), the question arises what is the physical mechanism for the troposphere-to-stratosphere transport (TST) that lifts air parcels (AP) from the main convective outflow around 350 K across the TTL into the lower stratosphere. The typical time scales for this transport, as derived from the upward propagation of the the seasonal cycle of CO_2

arising in the planetary boundary layer, vary between 2 and 3 month for the upward transport from θ=350 K up to 390 and 420 K, respectively (Andrews et al., 1999).

It is generally believed that the radiative heating effectively lifts AP within the TTL above Q=0 level where the background clear sky heating rate changes from a net cooling below to a net heating above. This transition level was generally found at an almost constant value of θ =360 K (≈15 km) (Gettelman et al., 2002). The transition from radiative cooling to radiative heating is driven by the combination of a rapid decrease in water vapor mixing ratios (longwave cooling is negligible above 360 K), suppressed longwave emission from CO_2 and ozone due to extremely cold temperatures and an increase of shortwave heating above 360 K owing to enhanced ozone mixing ratios.

Although, this explanation is widely subscribed, there remain aspects of TST that are not adequately addressed, e.g.: how do AP overcome the vertical gap between the main convective outflow around 350 and the level with significant heating rates. Normally, AP within the outflow region of the convective towers sink due to radiative cooling rather than ascend into the stratosphere. Clouds in the TTL tend to increase the potential temperature where Q=0 occurs due to suppressed longwave heating of the earth above clouds (Doherty et al., 1984; Gettelman et al., 2002). Consequently clouds increase the gap between the convective outflow and radiation driven transport by up to ≈25 K. Recently, Corti et al. (2006) proposed a new radiation-based mechanism showing that lofting via cirrus cloud-radiation has the potential to overcome this gap but there are still neither experimental evidences nor 3-D transport studies driven by realistic winds and cirrus cloud distributions which would support this theory.

Here, we propose an alternative mechanism for TST across the TTL mainly based on mixing in this region as diagnosed by the Chemical Lagrangian Model of the Stratosphere (CLaMS) (McKenna et al., 2002; Konopka et al., 2004). We show that the concept of deformation-induced mixing driven by large-scale meteorological winds as implemented in CLaMS identifies the TTL as a region with enhanced horizontal and vertical gradients in the horizontal wind, i.e. with increased horizontal shear and vertical strain rates, mainly occurring in the outflow of large-scale convection and in the

vicinity of the STJ.

Enhanced small-scale turbulence and mixing generated by shear induced by gravity waves can form in the large scale flow as was observed around the jet stream (Pavelin and Whiteway, 2002). Additionally regions with enhanced shear and strain rates can be diagnosed in terms of enhanced Lyapunov exponents (Pan et al., 2006) which, in turn, lead to increased mixing in the CLaMS parameterization, in particular to enhanced vertical mixing. This shear driven mixing offers an alternative mechanism for the TST across the TTL.

The paper is organized as follows: In the next section we describe the newly improved version of CLaMS. In this new version, the stratospheric CTM is extended through hybrid coordinate to the surface, incorporating the entire troposphere. To validate this new version, we use in situ observations on-board of the high altitude Russian aircraft Geophysica during the TROCCINOX (Tropical Convection, Cirrus and Nitrogen Oxides Experiment) campaign in early 2005 in Brazil that is shortly described in Sect. 3. In particular, to validate both STT and TST we compare in Sects. 4 and 5, respectively, the simulated tracer distributions with data obtained during two long-range flights penetrating the TTL. In Sect. 6 we discuss the contribution of mixing to the transport across the TTL and, finally, conclusions are drawn in Sect. 7.

2 Model description: CLaMS with stratosphere and troposphere

To resolve transport processes in the troposphere, in particular within the TTL, the vertical coordinate of CLaMS was extended from the potential temperature θ, to a hybrid pressure-potential temperature coordinate ζ (Mahowald et al., 2002). In this section, we describe some details of this extension with the main focus on implications for the vertical transport, in particular in regions affected by convection and by the STJ.

2.1 Hybrid vertical coordinate

Following the equations proposed by Mahowald et al. (2002), we generalize the potential temperature θ, to a hybrid coordinate ζ, that below a certain pressure level p_r approximating the tropopause (i.e. for pressure values $p>p_r$) smoothly transforms from isentropic to pressure coordinates:

$$\zeta(p) = f(\eta)\theta(p, T(p)), \quad \eta = \frac{p}{p_0} \tag{1}$$

with

$$f(\eta) = \begin{cases} \sin\left(\frac{\pi}{2}\frac{1-\eta}{1-\eta_r}\right) & \eta > \eta_r \\ 1 & \eta \leq \eta_r, \quad \eta_r = \frac{p_r}{p_0} \end{cases} \tag{2}$$

and $\theta=T(p_0/p)^{\kappa}$, $\kappa=0.286$. Here, T denotes the temperature, $p_0=1013$ hPa is the surface pressure and $p_r=100$ hPa was chosen. This pressure level roughly corresponds to the pressure at the tropical tropopause.

The ζ-coordinate is illustrated in the left panel of Fig. 2.

Here, as an example, the isolines of the zonally averaged pressure p (black) and potential temperature θ (orange) were calculated for one particular ECMWF data set (1 January 2004, 12:00 UT) and plotted as a function of latitude and the hybrid coordinate ζ. Above approximately $\zeta=380$ K, the θ-isolines and the ζ-coordinates are the same, whereas the p–isolines cross the ζ–levels. Contrary, below about $\zeta=300$ K, the p and ζ levels tend to become parallel to each other (even if the units of ζ are Kelvin), whereas the isentropes cross these lines. The $\zeta=0$ level exactly corresponds to $p=p_0$. The black region is confined by the $\zeta=0$ level and the highest values of the orography within each latitude bin (e.g. the highest point corresponds to the location of Mount Everest).

2.2 Entropy-preserving vertical distribution of AP

Unlike Eulerian CTMs, CLaMS considers an ensemble of AP on a time-dependent irregular grid (McKenna et al., 2002; Konopka et al., 2004, 2005). The initial positions of the AP have to be specified both in the horizontal and vertical. For a given horizontal resolution, i.e. the mean horizontal separation r_0 between adjacent AP, their mean vertical separation is, at first, a free parameter.

The layerwise mixing concept in CLaMS (i.e., the deformation-induced mixing is applied layerwise, with each layer containing approximately the same number of AP) requires that a grid of vertical layers, each with the thickness $\Delta\zeta$, has to be defined. Generally, $\Delta\zeta$ depends on ζ. In every layer, the AP are approximately uniformly distributed over the layer thickness $\Delta\zeta$ and, consequently, the mean vertical separation between the AP is given by $\Delta\zeta/2$. The dependence of $\Delta\zeta$ on ζ is motivated by the following ideas:

The ratio between the mean horizontal and vertical distance between the adjacent AP in a given layer $\Delta\zeta$, the so-called aspect ratio α, controls not only the spatial resolution in CLaMS but also the horizontal and vertical diffusivities if the AP being considered are involved in a mixing event. These diffusivities are proportional to r_0^2 and $\Delta\zeta^2/4$, respectively. Thus, an appropriate choice of α guarantees that the ratio between the horizontal and vertical diffusivity is correctly described. Furthermore, if α is correctly set, it also guarantees that the horizontal and vertical resolution of the model are consistent i.e. the tracer variability is resolved, both horizontally and vertically, to the same degree.

Haynes and Anglade (1997) derived from observations and theoretical estimates that α=250 is a good choice for the lower stratosphere. Using this value and the potential temperature as the vertical coordinate, CLaMS simulations, mainly in the lower stratosphere, could successfully reproduce the observed small-scale structures as filaments, vortex remnants or tracer gradients across the vortex edge (Konopka et al., 2003, 2004; Grooß et al., 2005).

Because the assumption of α=const cannot be applied for the troposphere (where much stronger vertical mixing is expected than in the lower stratosphere) and for the middle and upper stratosphere (where only an increase of the vertical diffusivity with altitude can explain the observed profiles of the stratospheric age Ehhalt et al., 2004), we need an additional criterion to create the grid of vertical layers, in particular if the CLaMS domain extends from the earth surface up to the stratopause.

Here, we propose that the "volume" of every AP should contain "the same amount of information" or, because the number of AP in each layer is approximately the same, we require a constant "amount of information" per layer, i.e. the total entropy of the layer ΔS should be constant. The latter one can be derived from the entropy density S defined as (Holton, 1992):

$$S \sim c_p n \ln \frac{\theta}{\theta_0} \tag{3}$$

with the specific heat c_p, air density n, potential temperature θ and the reference potential temperature θ_0. Using θ and n profiles of the U.S. standard atmosphere, $S(\zeta)$ calculated from (3) is plotted in the right panel of Fig. 2 (black) showing a clear maximum around 15 km. This is because θ increases while n decreases with the altitude (or with ζ) and, consequently, $S(\zeta)$ that is proportional to $n \ln \theta$, has a maximum.

Thus, in the new version of CLaMS, the vertical grid of layers is defined in the following way (see left panel of Fig. 2 where such layers are colored alternating with gray and white): first, for a given horizonal resolution r_0 and aspect ratio α (here α=250), a layer in the lower stratosphere with a thickness $\Delta\zeta = \alpha r_0$ is created. The total amount of entropy ΔS in this layer defines the thickness of all other layers by requiring ΔS=const in each layer. Using this condition and the entropy density S calculated for the U.S. standard atmosphere, a variable vertical spacing of layers is defined. An example is shown in Fig. 2 where r_0=200 km was specified. Note that the vertical grid with the thinnest layer around the tropical tropopause implies also the lowest vertical diffusivity per mixing event within this layer and that this diffusivity increases both above and below this level (red line on the right side of Fig. 2). The upward increase by about a factor

of 10 near 30 km is in a qualitative agreement with the expected relative increase of the vertical diffusivity as derived from the investigations of the age of air and of (one-dimensional) eddy diffusion coefficients (Ehhalt et al., 2004).

2.3 Hybrid vertical velocity

An important advantage of the ζ–coordinate is that it allows to couple the vertical velocities in the troposphere as implemented in the meteorological data, in particular the large-scale, convection-driven transport in the tropics, with the radiation-driven vertical velocities in the stratosphere. Thus, as in the previous version of CLaMS, the isentropic and cross-isentropic advection in CLaMS above the tropopause is driven by ECMWF winds and heating/cooling rates derived from the Morcrette scheme (clear sky conditions), respectively (Morcrette, 1991; Zhong and Haigh, 1995).

Below the tropopause, where the ζ–coordinate behaves like a pressure coordinate, the ECMWF vertical p-velocity ($\dot{p}$) is used which, within the ECMWF model, is derived from the continuity equation (Simmons et al., 1999). Strong updrafts due to enhanced values of $\dot{p}$ were found in the ECMWF analysis in regions where large-scale convection as those organized in the mesoscale convective systems (MCS) occurred (e.g. Hegglin et al., 2004). Following Mahowald et al. (2002), the time derivative of ζ follows from eq. (1):

$$\dot{\zeta} = \frac{d\zeta}{dt} = \dot{f}\theta + f\dot{\theta} \tag{4}$$

with

$$\dot{f} = \begin{cases} \frac{\pi}{2}\frac{\dot{\eta}}{\eta_r - 1}\cos\left(\frac{\pi}{2}\frac{1-\eta}{1-\eta_r}\right) & \eta > \eta_r \\ 0 & \eta \leq \eta_r \end{cases} \tag{5}$$

and $\dot{\eta}=\dot{p}/p_0$, where $\dot{p}$ is the vertical velocity in pressure coordinates (here provided by ECMWF) and $\dot{\theta}$ is derived from the Morcrette scheme. Generally, the first term in Eq. (4) dominates the second in convective regions. When $\dot{p}$ is negligible (e.g. away

from convective regions), Eq. (4) reduces to $\dot{\zeta}=f\dot{\theta}$. Thus, for p_r=100 hPa (as used here), the factor f decreases from 1, to 0.97, and 0.9 at p=100, 200 and 300 hPa, respectively, guaranteeing that radiation, i.e. $\dot{\theta}$, dominates the vertical velocities in the TTL in regions not affected by convection.

A new aspect of transport arises below the tropopause, where enhanced values of $\dot{\zeta}$ are dominated by large-scale convection. To illustrate this, we show, as an exemple, in the two top panels of Fig. 7

how a fast vertical transport can be diagnosed from the backward trajectories starting from the ζ=340 K surface (i.e. $p\approx$180 . . . 220 hPa) on 8 February 2005, 12:00 UT (there is no preference for this apart from the fact that it coincides with a Geophysica flight that will be discussed below).

Here, the elapsed time until a trajectory descended below p_c=500 (top panel) and p_c=300 hPa (middle panel) defines the time scale of this upward transport. This time allows the identification of regions where strong updraft in the last 120 h have occurred. In the following, we denote this time as the age of convection. Thus, between Indonesia and south-eastern Pacific (black arrows) an updraft of $\Delta p\approx$300 hPa in the last 24 h was found (top) while over Brazil, Central Africa and Madagaskar regions with $\Delta p\approx$100 hPa could be identified (middle).

Now, we compare these signatures of large-scale convection with the analyzed ECMWF specific humidity (H_2O) distribution (bottom panel of Fig. 7). The ECMWF H_2O distribution is a result of a 3-D variational analysis (3D-Var) combining the radiosonde and satellite observations with transport calculations constrained by the six-hourly analysis of wind and temperature (Simmons et al., 1999). The vertical transport of H_2O in the ECMWF model is driven not only by the p-velocity $\dot{p}$ but, in addition, by sub-scale convective transport based on the Tiedtke (1989) parameterization. Furthermore, condensation and evaporation processes shift water between the gaseous, liquid and solid states.

Thus, the spatial distribution of the enhanced H_2O values in the upper troposphere can be understood as a proxy for the fresh impact of convection. In particular, between

Indonesia and south-eastern Pacific (black arrows) this distribution correlates fairly well with the large-scale, deep convection derived from pure trajectory calculations indicating that large-scale convective patterns, probably caused by MCS, are well represented by $\dot{\zeta}$.

Finally, to illustrate the typical meridional and vertical dependence of $\dot{\zeta}$, its zonally and monthly averaged values calculated for March, June, September and December 2003 are shown in Fig. 4.

The vertical axis is rescaled by use of the entropy function $S(\zeta)$ (see Fig. 2, right panel), so the entropy density does not change along the vertical axis. In this way, the tropopause region is expanded relative to the troposphere and to the stratosphere. The gray contour defined by $\dot{\zeta}$=0 separates the regions with positive (ascent) from regions with negative values of $\dot{\zeta}$ (descent). The position of the tropopause (blue lines) is inferred from the |PV|=2–4 isolines in the extratropics and θ=380 K in the tropics. The p- and θ-isolines (black and pink) define the physical coordinates whereas $\zeta=\theta$ is valid only in the stratosphere.

Thus, in the tropics, above θ=360 K, the radiatively driven ascent determines the vertical velocities (ascending branch of the Brewer-Dobson circulation), whereas connectively-driven transport within the Hadley circulation (red and blue regions near equator) determines the vertical velocities below θ=340 K. In the polar regions during the winter, increased diabatic descent above 10 hPa indicates the positions of the polar vortices.

The meridional positions of the jets can be deduced from the isolines of the wind (white, solid – westerlies, dashed – easterlies) with a clear signature of STJ (maxima around ζ=360 K) and of the polar jets in the middle stratosphere during the winter. Below the tropopause in the extratropics, the signatures of the Ferrell cells can be seen which are driven by zonally asymmetric eddies along the poleward flanks of the STJ which dominate the extratropical circulation (e.g. Holton, 1992). The upward velocities in the Ferrell cells reach the extratropical tropopause (the gray contours defining $\dot{\zeta}$=0 cut the blue |PV|=2–4 PVU lines), although this ECMWF-based vertical transport

is probably too strong (see $\dot{\zeta}=0$ isoline on the SH in September in Fig. 4 extending up to 100 hPa). Thus, in the extratropics, p_r values higher than 100 hPa seem to be more appropriate for the transition level from the radiation- to ECMWF-related vertical velocities.

2.4 Mixing

As with the previous CLaMS version, the initial distribution of AP are transported according to trajectories calculated from horizontal ECMWF winds and vertical velocities $\dot{\zeta}$ with subsequent layerwise mixing. The mixing procedure uses the same optimized mixing parameters as described in Konopka et al. (2004) (critical Lyapunov exponent λ_c=1.5 day^{-1}) and is applied after each advection step Δt=24 h. The critical deformation associated with this advection step is given by $\gamma_c=\lambda_c\Delta t$=1.5. Thus, flow deformations with $\gamma>\gamma_c$ effectively trigger mixing within CLaMS. This spatially and temporally inhomogeneous procedure is driven by strain and shear rates of the horizontal wind with highest values in the vicinity of the jets, in particular in the outer flanks of the polar jet (Konopka et al., 2004, 2005) or in the vicinity of the STJ (Pan et al., 2006).

Now, we discuss how CLaMS mixing works within the TTL. In the three panels of Fig. 7, the mean vertical diffusivity D_v per AP is shown for ζ=340, 360, 380 K from top to bottom, respectively (blue shaded), as parameterized by the CLaMS mixing algorithm applied on 8 February 2005, after the last advection step. D_v for each AP involved into the mixing procedure is given by $D_v \approx \Delta z^2/4\Delta t$ and set to 0 if AP was not affected by mixing. The mean values of D_v are derived from the fraction of AP affected by mixing within the grid box with 100 km length. Δz is the geometric thickness of the considered level $\Delta\zeta$. D_v varies between 0 (white) and $\approx$1 m^2/s (dark blue).

The contours of the horizontal wind u (red) highlight the position of the STJ, with highest values at ζ=340 and with a stronger jet in the winter NH (u>60 m/s) than in the summer SH. The yellow isolines show regions with enhanced absolute values of the vertical shear, $|du/d\zeta|$, derived from the difference of the horizontal wind in the layer

above and below the considered layer. Thus, increased values of D_v (dark blue) can be found in regions with enhanced horizontal velocity (jets) or enhanced vertical shear (tropics or jets). The highest values of vertical shear are diagnosed above the core of the NH STJ at ζ=380 K or in the outflow regions of tropical convection at ζ=360 K. The latter can be found e.g. above south-eastern Pacific, downwind of 24 h isolines of the age of convection as can be seen in Fig. 7 (black arrows).

Both, horizontal strain and vertical shear are sources of deformations in the flow (high Lyapunov exponents, not shown) which trigger the mixing algorithm in CLaMS. Whereas the signature of mixing at ζ=380 K coincides well with the position of the jets, high vertical diffusivity values at 340 and 360 K in the tropics correlate to some extent with the locations where convection was diagnosed. A detailed analysis of the Lyapunov exponents shows that increased vertical shear rates in the large-scale convective outflow regions also cause high mixing rates in CLaMS.

The pattern of the horizontal diffusivity D_h is approximately the same as that of the vertical diffusivity D_v. With $D_h=\alpha^2 D_v$ and α=250 (Haynes and Anglade, 1997; Konopka et al., 2005), D_h is approximately by a factor 10^4 larger than D_v around the tropical tropopause. Because α decreases with the distance from the ζ=380 K level, the corresponding values of D_h are also smaller. Thus, CLaMS transport in the TTL shows high mixing rates in the vicinity of the STJ and in the outflow regions of the large-scale convection, i.e., these locations are favored for the mixing-induced vertical transport across the TTL.

2.5 Boundary conditions

In addition to the initial conditions that will be described in the next section, boundary conditions need to be specified for the CLaMS model domain. After each mixing procedure, the AP in the top level of the model are replaced by their initial geometric configuration. Furthermore, the mixing ratios are set to prescribed values as given by the HALOE climatology, Mainz-2D model or by some additional conditions

(e.g. tracer-tracer correlation, e.g. Grooß et al., 2005). Also the AP with $\zeta_0<\zeta<\zeta_0+\Delta\zeta_0$ with $\Delta\zeta_0$=50 K and ζ_0 defined by the surface that follows the orography at the bottom of the model domain are replaced be their initial geometric positions. Their mixing ratios are either redefined in a similar way as for the upper boundary or are interpolated from their next neighbors and can be updated, e.g. according to prescribed fluxes.

3 Validation of CLaMS transport by TROCCINOX measurements

To validate the properties of transport associated with the new hybrid coordinate ζ, we use in situ data measured during the TROCCINOX campaign on-board of the high altitude Russian aircraft Geophysica. The campaign took place in early 2005 in Araçatuba (21.2° S, 50.4° W), Brazil with 8 local and 7 transfer flights extending up to 20 km (or up to $\theta\approx$450 K), i.e. well-covering the TTL region.

The experimental data used in this paper were sampled with FOZAN (ozone), FISH (total and gas phase water), HAGAR (CH_4), SIOUX (NO, NO_y) and COLD (CO) instruments. A detailed description of the instruments can be found in Stefanutti et al. (2004) and Voigt et al. (2004) for the SIOUX instrument.

3.1 Meteorological situation

The composition of tropical air in the vicinity of the tropopause over Araçatuba was frequently influenced by the interaction between the upper-level, quasi-stationary Bolivian high (BH) with STJ (see Fig. 6)

surrounding the BH southerly. Zhou and Lau (1998) have reported the existence of high-level southerlies over South America during the austral summer, which were influenced by the BH, and pointed out some similarities of this circulation pattern with the well-known summer monsoon circulation over south-east Asia (e.g. Dethof et al., 1999). The air over Araçatuba was influenced by numerous MCS that frequently formed over the southeast of South America (north Argentina, south Brazil, part of Paraguay and

part of Uruguay). These air masses were transported along the STJ, often displaced by the high-level southerlies, to a region within the Geophysica range. In addition, isolated thunderstorms in the vicinity of Araçatuba were also observed by the Brazilian radar network.

The eight local flights performed during the campaign can be divided into 3 groups: 4 flights in almost pure tropical air, northwards of the STJ on 12, 15, 17 and 18 February, 2 flights above and within isolated thunderstorms on 4 and 5 February, and 2 flights on 1 and 8 February in air masses strongly affected by the aged MCS and STJ. Because in contrast to the MCS, the isolated convective systems such as those on 4 and 5 February are not resolved by the ECMWF large-scale analysis, we focus our analysis on the flight on 1 February for stratosphere-troposphere transport (STT) and on 8 February for the reverse transport (TST) (Fig. 6 top and bottom). But first, we describe the setup of CLaMS used for this study.

3.2 Configuration of CLaMS

The high resolution (50 km horizontally and up to 200 m vertically around the tropical tropopause) version of CLaMS as described in the previous section is used to transport O_3 and N_2O as passive tracers without any chemical change. The model was initialized globally, between the earth surface and ζ=1400 K, for 20 November 2004, using MLS observations and Mainz-2D model above and below ζ=400 K, respectively (Grooß et al., 2005).

Two artificial tracers are used to mark air masses with different origins. In particular, the stratospheric tracer (ST) is set to 100% at the initialization time in the domain defined by ζ>380 in the tropics (i.e. within the latitude range between 20° S and 20° N) and by |PV|>2 elsewhere. At the top CLaMS level, ST is held constant during the entire simulation. The ST value of a given AP can change only due to mixing and, consequently, this value quantifies the percentage of stratospheric air within this air mass. Similarly, the boundary layer tracer (BL) is re-initialized every 24 h to 100% within the lowest layer with the thickness $\Delta\zeta$=50 K that follows the orography. Thus,

high BL values in the upper troposphere indicate a fast vertical transport driven by convection.

To understand the impact of mixing on the transport of species we run CLaMS in two configurations: without mixing (i.e. transport only in terms of forward trajectories) and with mixing by using mixing parameters described in Sect. 2.4.

4 Stratospheric intrusion into the TTL

During the flight on 1 February, tracer signatures of a deep stratospheric intrusion into the TTL were observed. This intrusion (cut-off low) was formed as a tongue of low PV (see Fig. 6, top panel) that had been separated from the stratosphere and transported on a time scale of several days into the TTL by a meandering and relatively weak STJ. Occasionally, the meandering STJ that surrounds the BH becomes unstable (usually when the BH is displaced eastwards) and bifurcates into two branches. Whereas the main branch follows the main eastward direction, a secondary branch flows anticlockwise around the BH and mixes into the TTL.

Along the flight track (Fig. 7, top panel), enhanced ozone values (black arrows) were observed several times by the FOZAN instrument (black)

clearly below the tropopause (defined here as |PV|=2 PVU surface). These signatures could be successfully reproduced with CLaMS (colored line), with a better agreement than the assimilated ozone provided by ECMWF (pink). The colors of the CLaMS line denote the percentage of the stratospheric tracer ST. CLaMS results with mixing switched off (gray) strongly overestimate the observed ozone values, in particular below the tropopause indicating to weak upward (or to strong downward) transport in pure trajectory studies.

The vertical ST distribution above and below the flight track together with |PV|=2 PVU (tropopause) and Q=0 (clear sky radiative equilibrium) are shown in the left bottom panel of Fig. 7. The spatial distribution of ST extends down up to about 500 hPa. The position of the meandering STJ (see also Fig. 6) can be inferred from the iso-

tachs of the horizontal wind (light gray). A strong STT signal observed during this flight can also be seen in the comparison of the ozone profiles with all other profiles measured during the campaign (right bottom panel of Fig. 7). The profiles measured on 1 February which are also colored with ST, show strong stratospheric signatures around ζ=250 K (≈500 hPa) with ozone values around 100 ppbv (black arrow). This is significantly higher than all other tropospheric ozone values measured during the campaign (gray lines).

To some extent, the jet still isolates stratospheric intrusion from the tropical air while the remnants of this intrusion are mixed into the troposphere, mainly below the jet. A good agreement between the observed and simulated filaments (black arrows in the top panel of Fig. 7) and the position of the ST remnants shows the ability of CLaMS to reproduce small-scale structure within the TTL.

An overall good agreement between the simulated and observed O_3 and CH_4 time series could be achieved for all local flights with correlation coefficients 0.89 and 0.86, respectively. The passively transported O_3 slightly underestimates the observed values in the lower stratosphere indicating that chemical ozone production as expected in the tropics might improve the agreement in full chemistry studies. Ozone assimilated by ECMWF overestimates the FOZAN observations above θ=380 K, with a linearly increasing error up to 40% at θ=450 K.

5 Troposphere-to-stratosphere transport along the subtropical jet

The flight on 8 February, permits the study of the reverse process namely the transport of tropospheric air into the TTL. During the outbound flight leg between 13:45 and 15:30 UT, the TTL was penetrated around θ≈360 K (see Fig. 6, bottom panel). The considered flight leg starts slightly below the |PV|=2 VU surface over Araçatuba and leads toward the STJ core around the easternmost point of the flight track with |PV|>3 PVU and wind velocities higher than 35 m/s (see also Fig. 12).

Along this leg (see Fig. 8),

signatures of pure tropospheric and mixed, i.e. of tropospheric and stratospheric influence were found in the beige (AB) and green (BC) colored time intervals, respectively. In particular, enhanced values of total water (up to 30 ppmv, yellow) and water vapor (up to 15 ppmv, blue) were detected by FISH instrument at pressure level 125 hPa, i.e. slightly above θ=360 K. A positive difference between the total water and water vapor indicate the existence of cirrus clouds. This signature can be seen twice, shortly before 14:00 and a small spike after 15:00 UTC.

Surprisingly, after about 14:30 UT (BC), enhanced ozone values (up to 150 ppbv, FOZAN) were detected (black), indicating increasing stratospheric influence. This transition from the tropospheric to stratospheric O_3 mixing ratios is also reproduced by CLaMS simulations with mixing (red). On the other hand, pure trajectory calculations (gray) significantly overestimate the observed ozone values showing that such calculations do not correctly represent the upward transport.

The simultaneous presence of the tropospheric and stratospheric signatures in the air masses observed on 8 February (and 1 February) can also be seen in Fig. 9

where the profiles of the total water (a) as well as the correlations of ozone with total water (b) and NO/NO_y (c) are compared with other pure tropical flights (black versus gray) or with the flight on 1 February (violet). Thus, significant higher values of H_2O were observed within the TTL affected by the STJ (black and violet) than within the tropical TTL far away from the STJ (gray). In particular, as can be deduced from the ozone/total water correlation, the air masses sampled along the entire ABC leg were influenced by mixing between the troposphere and stratosphere (relatively strong deviation of the observed correlations from an ideal, unmixed, L-shaped correlation) with much higher stratospheric influence along the BC than along the AB part of the leg.

Furthermore, comparatively high ratios of NO/NO_y (30–55%) were observed along the entire ABC segment that indicates contributions of relatively fresh lightning. Based on observations around 200 hPa, Schumann et al. (2004) report that ratios between 30 and 50% are signatures of lightning not older than 3 h. Because the lifetime of NO_x

at 125 hPa is by about a factor 10 longer than at 200 hPa (Tie et al., 2001, 2002), the observed NO/NO_y ratios may be typical for an elapsed time of the order of few days. Using trajectory analysis, we discuss now the the origin of these air masses.

5.1 Trajectory analysis

A common way to trace back the origin of the sampled air masses, is to use backward trajectories starting from the flight track (see Fig. 10, top panel). Here, the positions and the ECMWF H_2O mixing ratios along 3-days backward trajectories are shown. The trajectories were calculated using ζ-coordinates and the CLaMS trajectory module driven by the 6-h ECMWF analysis data.

The trajectories show high ECMWF H_2O values of about 50 ppmv about 30 h before the flight whereas about 40 h prior the flight H_2O values less than 7 ppmv were found in these air masses. Furthermore, the potential temperature did not significantly change along these trajectories (the absolute variation is smaller than 2 K) indicating an almost isentropic transport. Because the trajectories do not descend below ≈200 hPa, the diagnosed high ECMWF H_2O values are probably caused by the sub-grid parameterization of convection in the ECMWF model.

Similar results were also found with the FLEXPART model (Ren et al., 2006[1]) and with LAGRANTO trajectories driven by 3-h ECMWF data (Wernli and Davies, 1997), even if some of those backward trajectories reached ≈220 hPa level. Furthermore, for all flight legs on 1, 4, 5 and 8 February with $350<\theta<380$, the corresponding backward trajectories, calculated both with CLaMS and LAGRANTO, do not descend below ≈300 hPa for the previous 5 days, even on 4 and 5 February when the observed air masses were strongly influenced by fresh convection. The small discrepancies between CLaMS and LAGRANTO likely originate from the differences in the applied

[1]Ren, C., MacKenzie, A. R., and Schiller: Diagnosis of processes controlling water vapour in the tropical tropopause layer by a Lagrangian cirrus model, Atmos. Chem. Phys. Discuss., submitted, 2006.

ECMWF data (6 versus 3-h frequency) rather then from the differences in the trajectory advection schemes.

The vertical displacement of the backward trajectories changes significantly if their start positions are shifted down below the flight track by 25 K.

In the bottom panel of Fig. 10, the horizontal coordinates of the 3-days backward trajectories are shown, which were initialized 25 K below the flight leg ABC on 8 February (i.e. 25 K below the beige and green time segments). The positive (negative) values of $\Delta\theta$ along the trajectories denote their total ascent (descent) with increasing time. The gray footprints show the positions where these trajectories crossed the 400 hPa level and, in the following, these positions are interpreted as regions where convection lifted the corresponding air masses. The age of convection can be derived from the trajectory length (see legend in Fig. 10) and varies between 30 and 70 h for the southern- and westernmost footprints, respectively.

Such interpretation of the footprints is supported by the infrared (chanel 4) GOES-East satellite pictures (Fig. 11),

which show a convective cloud covering 53, 40 and 30 h before the flight at approximately the same locations as inferred from trajectory calculations. Thus, it seems that two MCS, the older one over northeast of south of Brazil and part of Uruguay (beige) and the younger one over Argentina (green), contributed to the tropospheric signatures in the respective AB and BC parts of the considered flight leg. A different origin of these air masses manifests also in a discontinuity in the measured time series of water vapor around 14:30 UT (see Fig. 8). This discontinuity can also be seen in the time series of temperature (first part of the leg is colder by ≈3 K) and the relative humidity (not shown).

5.2 Contribution of mixing

Thus, the question arises what is the reason that trajectory analysis can explain the convection-induced tropospheric signatures at most up to $\theta \approx 340$ K but not the observed relatively fresh tropospheric signatures (enhanced NO/NO_y ratio and cirrus

clouds) found slightly above 360 K? As a first hypothesis, it is possible that $\dot{\zeta}$ derived from the large-scale ECMWF p-velocity underestimates the vertical velocities in regions affected by convection.

To some extent this hypothesis is supported by observations of CO by the COLD instrument on 4 February with maximum mixing ratio of ≈140 ppbv extending up to about 360 K in air masses within and slightly above an isolated convective cell (unfortunately, there are no observations of CO on 1 and 8 February and the quality of the CLaMS CO distribution is strongly limited by a very uncertain data-base of CO sources, in particular in South America). Within CLaMS, the highest impact of convection can be defined as the highest level reached by undiluted values of the BL tracer (i.e. ≈100%). For all flights when CO was available, this level was found by about θ=350 K, i.e. about 10 K below the highest convective outflow derived from CO observations.

However, the underestimation of the convective outflow by $\Delta\theta$≈10 K does not completely explain the discrepancy between the backward trajectory analysis that started 25 K below the flight level and the observed, relatively fresh tropospheric signatures at ≈360 K. In the remaining part of this section, we show that mixing, in particular as those implemented in CLaMS, has the potential to close this gap.

To explore this hypothesis, an additional CLaMS simulation was performed, with BL tracer re-initialized 3 days before the flight to 100% and 0 above and below 400 hPa, respectively. In this way, we redefine the boundary layer tracer BL to a tropospheric tracer and ask if during the following 3 days, convection and mixing can lift this tracer up to about θ=360 K. The results are plotted as a curtain along the flight track in Fig. 12.

Here, the BL tracer extends well above the θ=335 K, i.e. well above the maximum of the upward transport as inferred from the pure trajectory analysis shown in Fig. 10. In particular the BL signature extends up to the AB part of the leg around 14:00 UT (beige), but never reaches the BC part of the leg (green) getting no closer than 10 K below the flight level at 14:45 UT. The position of the first BL signature (beige arrow) roughly coincides with the position of the cirrus clouds.

In addition, the distribution of the ST tracer (not shown) that can be approximated

by ST≈100%-BL coincides with the increasing stratospheric properties of the sampled air masses as the Geophysica comes closer to the STJ (illustrated here by the isotachs of the horizontal wind, light gray). The aircraft cross the |PV|=2 PVU tropopause around 14:00 UT (the violet line denotes the tropopause in Fig. 10), with an increasing stratospheric character of the sampled air along the BC part of the flight leg. Thus, in agreement with observed and simulated O_3 time series (Fig. 8), the stratospheric contribution increases during the considered flight leg as the Geophysica approaches the jet core. At the end of the second part of the leg (point C), slightly above the PV-tropopause, BL and ST tracers transported over the entire period of 3 months show the weakest tropospheric impact and the strongest contribution of air originating in the lowermost stratosphere, respectively.

We conclude that vertical and isentropic mixing as implemented in CLaMS extend the pure trajectory calculations and explain, at least qualitatively, the observed signatures. In the following section, we discus some additional arguments supporting this hypothesis.

6 Mixing-driven transport in the TTL

To show that mixing in CLaMS does play a crucial role in lifting tropospheric air from the convective outflow around 350 K up to the tropical tropopause around 380 K, we discuss now in Fig. 13

the horizontal (top row) and zonally averaged vertical (bottom row) distributions of BL tracer after more than 3 months of transport (108 days) of transport with and without mixing. In the case without mixing, pure advective transport along trajectories occurs, which are calculated in ζ−coordinates, i.e. by the use of hybrid vertical velocities $\dot{\zeta}$. The horizontal distributions in the top row of Fig. 13 show AP within the layer around ζ=380 K. The beige lines are the isotachs of the total and zonal wind in the horizontal and vertical cross sections, respectively and illustrate the positions of STJ on the last day of the simulation period (i.e. on 7 March 2005). The blue lines in the bottom row

indicate the position of the tropopause and are inferred from the |PV|=2–4 isolines in the extratropics and θ=380 K in the tropics.

The large white gaps where AP are absent in the left top panel of Fig. 13 illustrate that insufficient number of AP ascend in the tropics, or, in other words, that the upward transport driven by convection (from ECMWF) and by radiation (clear sky) is too weak to transport tropospheric species up to the tropical tropopause at $\theta \approx \zeta$=380 K. By contrast, the full CLaMS simulations with mixing (right top panel of Fig. 13) show a clear, filamentary signature of upward transport within the tropics laterally confined between the northern and southern STJ and with highest BL values in the tropics over Indonesia and south of the equator over the western Pacific.

The zonally averaged vertical distribution of the BL tracer shown in the bottom right panel of Fig. 13 illustrates also a clear signature of mixing if compared with the results of a pure trajectory transport (bottom left). The vertical mixing strongly affects the TTL region above $\zeta \approx$360 K. Furthermore, a stronger convective activity and a weaker STJ in the summer hemisphere effectively fill the SH lowermost stratosphere with tropospheric air whereas in the NH a stronger STJ combined with an enhanced diabatic descent into the lowermost stratosphere hinder an effective TST.

The meridional distribution of the fraction of CLaMS AP affected by mixing and averaged over the entire simulation time is shown in the top panel of Fig. 14.

The white and gray lines denote the mean wind isotachs and the mean Q=0 line, respectively. The blue lines denotes the mean tropopause calculated as for Fig. 13. All these lines are derived from the meteorological data averaged over the entire simulation time of 108 days.

Thus, a stronger STJ in the NH is associated with a higher mixing intensity both below the jet and on its tropical side. Remarkably, the whole TTL, i.e. the region confined by the jets and θ-values between 350 and 420 K is affected by mixing even if the largest contribution can be found on the tropical side of the STJ. Note that convection in the tropics below $\approx$340 K is described in CLaMS as advective part of transport (i.e. in terms of trajectories and without mixing) and, consequently, does not significantly contribute

to CLaMS mixing.

It should be emphasized that our concept of mixing-driven transport, in particular in the vicinity of the jets, does agree with the general understanding of STJ as seasonally-dependent barriers for isentropic transport (Haynes and Shuckburgh, 2000). This effect that hinders horizontal transport of constituents from or into the TTL manifests in steep isentropic gradients of tracers perpendicular to the jet axis which form on a time scale of several weeks. This property can be seen in the meridional distribution of the BL tracer shown in the right bottom panel in Fig. 13 with a more permeable summer southern STJ in comparison to the northern STJ.

Although the highest mixing intensity in CLaMS is found on the tropical side of the winter STJ (see top panel of Fig. 14), such a jet, mainly due to a strong zonal orientation, serves as a very effective barrier for the isentropic transport. Conversely, a weak meandering summer STJ offers only a weak barrier for horizontal transport despite smaller mixing rates diagnosed in its vicinity. Thus, mixing through the barrier weakening the isentropic tracer gradients across the barrier does not necessary follow high local mixing rates diagnosed on both sides of the barrier. The winter (summer) STJ forms such a strong (weak) transport barrier. One has to distinguish two different features of transport: the net transport across the barrier occurring on a time scale of several weeks and the local mixing rates on both sides of such a barrier occurring on time scale of hours and homogenizing the tracer distributions separated by the barrier. Here, these two features are anti-correlated.

Furthermore, even if the mean lowest temperatures (thick black lines in Fig. 14) are symmetrically located over the equator, their position with respect to the jets is strongly asymmetric. Thus, despite a stronger vertical mixing at the tropical side of the NH STJ, water vapor can be more effectively condensed above this region than during the upward transport occurring in the vicinity of the SH STJ. This means that sufficiently strong convection interacting with the summer STJ seems to be a favored path for an effective upward transport of water vapor.

To some extent the enhanced mixing in CLaMS around θ=380 K results from the

necessity to fill the "white" regions in the left top panel of Fig. 13 with new AP (note that additional interpolations mean adding new AP that, consequently, means additional mixing in the model Konopka et al., 2004). This can be understood as a consequence of the violation of the continuity equation caused by the use of hybrid vertical velocities where approximately above 300 hPa the ECMWF vertical p-velocities (which fulfill the continuity equation) are gradually replaced by the vertical velocities calculated from the radiation scheme.

Because in the parts of the UT/LS region which are not affected by convection, the vertical velocities are, at least, by two orders of magnitude smaller than the horizontal wind, their values derived from the continuity equation are strongly affected by the limited accuracy of the horizontal wind. Typical horizontal and vertical velocities in the UT/LS region are of the order 10 and less than 0.01 m/s, respectively. Thus, horizontal wind accuracy higher than 1% would be necessary to resolve such small vertical winds.

This is the reason why most of the stratospheric CTMs like SLIMCAT (Feng et al., 2004) or CLaMS or trajectory-based studies in the stratosphere (Schoeberl and Newman, 1995; Rex et al., 1998) utilize vertical velocities calculated from a radiation scheme and why these velocities in the UT/LS region if derived from the horizontal wind via continuity equation are used only in statistical sense, e.g. in terms of monthly averaged values (Norton, 2002) or by appropriate climatology of trajectories (Stohl, 2000; Fueglistaler et al., 2004).

In the bottom panel of Fig. 14 the mean residual R of the continuity equation in ζ-coordinates (i.e. mainly the divergence of the velocity field) averaged over the simulated period is shown (see Holton, 1992, Eq. 4.31 with $\sigma = -g^{-1}\partial p/\partial\zeta$). High absolute values of R identify regions where the velocity field does not fulfill the continuity equation. In particular, strong negative values of R as diagnosed in the TTL region (Fig. 14) are caused by too weak upwelling or too strong poleward transport.

In CLaMS the diffusive flux lifts tropospheric air into the stratosphere across the TTL. In contrast to Eulerian models where (numerical) mixing in form of numerical diffusion is proportional to the flow velocity, i.e. $D \sim \mathbf{u}$ (Courant et al., 1928), the Lagrangian

approach, in particular the implementation of mixing in CLaMS, allows to couple mixing with gradients of **u** (horizontal strain and vertical shear) which, generally, are believed to drive turbulence and mixing (Smagorinsky, 1963).

The high rates of such deformations within the TTL, in particular in the outflow of the large-scale convection and in the vicinity of the STJ, enhance the diffusive flux across the TTL. This occurs even if the continuity equation would be satisfied because the number of mixing events which are necessary to close the white gaps in the left top panel of Fig. 13 is only a small fraction (≈5%) of all the mixing events induced by the flow deformations.

To summerize, there are several options to reevaluate the transport processes in the TTL: either the mean convective outflow described in terms of the ECMWF large-scale vertical velocities is higher than 350 K and has to be parameterized by including sub-grid convection as discussed e.g. in Tiedtke (1989), or, the clear sky radiation has to be extended by accounting for the effect of thin cirrus clouds in the way proposed by Corti et al. (2006), or the mixing-driven transport as proposed in this paper is, at least, an additional mechanism that effectively lifts the air masses across the TTL.

7 Conclusions

The mixing-driven transport from the mean convective outflow across the TTL up into the stratosphere offers an alternative path for the troposphere-to-stratosphere transport (TST). Both the experimental data measured on-board of high altitude research aircraft Geophysica (ozone, water vapor, NO, NO_y, CH_4 and CO) in the altitude range spanning the TTL regions and the CLaMS studies with and without mixing strongly support this idea. The mixing-induced vertical transport occurs preferentially in regions with high shear and strain rates mainly found in the outflow of the large-scale convection and in the vicinity of the subtropical jets. Even when a strong winter jet acts as an effective barrier for isentropic transport, enhanced vertical transport can occur within its tropical flanks. Conversely, a weak summer jet can be characterized by a higher isen-

tropic permeability and a weaker vertical transport. TST seems to be most effective if the outflow of mesoscale convective systems which reach the region penetrated by the subtropical jet. In particular, the most effective upward transport of H_2O is expected in the subtropical summer hemisphere.

Acknowledgements. TROCCINOX was partially founded by the Commission of the European Community under contract EVK2-CT-2001-00122. The field experiment was performed with the Brazilian partner project TROCCIBAS, coordinated by IPMET (Insituto de Pesquisas Meteorologicas), Bauru, Sao Paulo, Brazil. The European Centre for Medium-Range Weather Forecasts (ECMWF) is acknowledged for meteorological data support. Excellent programming support was provided by N. Thomas. We are grateful for the contributions of D. Brunner and C. Schwierz providing us with the LAGRANTO trajectories. The authors wish to express their gratitude to the crew of the Geophysica, to all the technicians and co-workers who contributed to the successful execution of the campaign and, in particular, to U. Schumann the coordinator of TROCCINOX.

References

Andrews, A. E., Boering, K. A., Daube, B. C., Wofsy, S. C., Hintsa, E. J., Weinstock, E. M., and Bui, T. B.: Empirical age spectra for the lower tropical stratosphere from in situ observations of CO_2: Implications for stratospheric transport, J. Geophys. Res., 104, 26 581–26 595, 1999. 12220

Atticks, M. G. and Robinson, G. D.: Some features of the structure of the tropical tropopause, Q. J. R. Meteorol. Soc., 109, 295–308, 1983. 12219

Corti, F., Luo, B. P., Fu, Q., Vömel, H., and Peter, T.: The impact of cirrus clouds on tropical troposphere-to-stratosphere transport, Atmos. Chem. Phys., 6, 2539–2547, 2006. 12220, 12242

Courant, R., Friedrichs, K., and Lewy, H.: Über die partiellen Differenzengleichungen der mathematischen Physik, Mathematische Annalen, 100, 32–74, 1928. 12241

Dethof, A., O'Neill, A., Slingo, J. M., and Smit, H. G. J.: A mechanism for moistening the lower stratosphere involving the Asian summer monsoon, Q. J. R. Meteorol. Soc., 556, 1079–1106, 1999. 12230

Doherty, G. M., Newell, R. E., and Danielsen, E. F.: Radiative heating rates near the stratospheric fountain, J. Geophys. Res., 89, 1380–1384, 1984. 12220

Ehhalt, D. H., Rohrer, F., Schauffler, S., and Prather, M.: On the decay of stratospheric pollutants: Diagnosing the longest-lived eigenmode, J. Geophys. Res., 109, 347–350, 2004. 12224, 12225

Feng, W., Chipperfield, M. P., Davies, S., Sen, B., Toon, G., Blavier, J. F., Webster, C. R., Volk, C. M., Ulanovsky, A., Ravegnani, F., von der Gathen, P., Jost, H., Richard, E. C., and Claude, H.: Three-dimensional model study of the Arctic ozone loss in 2002/2003 and comparison with 1999/2000 and 2003/2004, Atmos. Chem. Phys., 5, 139–152, 2004. 12241

Folkins, I. and Martin, R. V.: The vertical structure of tropical convection and its impact on the budget of water vapor and ozone, J. Atmos. Chem., 62, 1560–1573, 2005. 12219

Fueglistaler, S., Wernli, H., and Peter, T.: Tropical troposphere-to-stratosphere transport inferred from trajectory calculations, J. Geophys. Res., 109, D03108, doi:10.1029/2003JD004069, 2004. 12241

Gettelman, A., Salby, M. L., and Sassi, F.: Distribution and influence of convection in the tropical tropopause region, J. Geophys. Res., 107(D10), doi:10.10029/2001jd000876, 2002. 12219, 12220

Grooß, J.-U., Günther, G., Müller, R., Konopka, P., Bausch, S., Schlager, H., Voigt, C., Volk, C. M., and Toon, G. C.: Simulation of denitrification and ozone loss for the Arctic winter 2002/2003, Atmos. Chem. Phys., 5, 2973–2988, 2005. 12223, 12230

Grooß, J.-U., Konopka, P., and Müller, R.: Ozone chemistry during the 2002 Antarctic vortex split, J. Atmos. Sci., 62, 860–870, 2005. 12231

Haynes, P. and Anglade, J.: The vertical scale cascade in atmospheric tracers due to large-scale differential advection, J. Atmos. Sci., 54, 1121–1136, 1997. 12223, 12229

Haynes, P. and Shuckburgh, E.: Effective diffusivity as a diagnostic of atmospheric transport, 2, Troposphere and lower stratosphere, J. Geophys. Res., 105, 22 795–22 810, 2000. 12219, 12240

Hegglin, M. I., Brunner, D., Wernli, H., Schwierz, C., Martius, O., Hoor, P., Fischer, H., Spelten, N., Schiller, C., Krebsbach, M., Parchatka, U., Weers, U., Staehelin, J., and Peter, T.: Tracing troposphere-to-stratosphere transport above a mid-latitude deep convective system, Atmos. Chem. Phys., 4, 169–206, 2004. 12225

Holton, J. R.: An Introduction to Dynamic Meteorology, Academic Press, London, 1992. 12224, 12227, 12241

Holton, J. R., Haynes, P., McIntyre, M. E., Douglass, A. R., Rood, R. B., and Pfister, L.: Stratosphere-troposphere exchange, Rev. Geophys., 33, 403–439, 1995. 12219

Kelly, K., Profitt, M. H., Chan, K. R., Loewenstein, M., Podolske, J. R., Strahan, S. E., Wilson, J. C., and Kley, D.: Water vapor and cloud water measurements over Darwin during the STEP 1987 tropical mission, J. Geophys. Res., 98, 8713–8723, 1993. 12219

Konopka, P., Grooß, J. U., Günther, G., McKenna, D. S., Müller, R., Elkins, J. W., Fahey, D., and Popp, P.: Weak impact of mixing on chlorine deactivation during SOLVE/THESEO2000: Lagrangian modeling (CLaMS) versus ER-2 in situ observations., J. Geophys. Res., 108, 8324, doi:10.1029/2001JD000876, , 2003. 12223

Konopka, P., Steinhorst, H.-M., Grooß, J.-U., Günther, G., Müller, R., Elkins, J. W., Jost, H.-J., Richard, E., Schmidt, U., Toon, G., and McKenna, D. S.: Mixing and Ozone Loss in the 1999-2000 Arctic Vortex: Simulations with the 3-dimensional Chemical Lagrangian Model of the Stratosphere (CLaMS), J. Geophys. Res., 109, D02315, doi:10.1029/2003JD003792, 2004. 12220, 12223, 12228, 12241

Konopka, P., Günther, G., McKenna, D. S., Müller, R., Offermann, D., Spang, R., and Riese, M.: How homogeneous and isotropic is stratospheric mixing? Comparison of CRISTA-1 observations with transport studies based on the Chemical Lagrangian Model of the Stratosphere (CLaMS), Q. J. R. Meteorol. Soc., 131, 565–579, 2005. 12223, 12228, 12229

Mahowald, N. M., Plumb, R. A., Rasch, P. J., del Corral, J., and Sassi, F.: Stratospheric transport in a three-dimensional isentropic coordinate model, J. Geophys. Res., 107, 2002. 12221, 12222, 12225

McKenna, D. S., Konopka, P., Grooß, J.-U., Günther, G., Müller, R., Spang, R., Offermann, D., and Orsolini, Y.: A new Chemical Lagrangian Model of the Stratosphere (CLaMS): Part I Formulation of advection and mixing, J. Geophys. Res., 107, 4309, doi:10.1029/2000JD000114, 2002. 12220, 12223

Morcrette, J.-J.: Radiation and Cloud Radiative Properties in the European Centre for Medium-Range Weather Forecasts Forecasting System, J. Geophys. Res., 96, 9121–9132, 1991. 12225

Norton, W. A.: Longwave heating of the tropical lower stratosphere, Geophys. Res. Lett., 28, 3653–3656, 2002. 12241

Pan, L. L., Konopka, P., and Browell, E. V.: Observations and Model Simulations of Mixing near the Extratropical Tropopause, J. Geophys. Res., 111, 2006. 12221, 12228

Pavelin, E. and Whiteway, J. A.: Gravity wave interactions around the jet stream, Geophys.

Res. Lett., 29, 2024, doi:10.1029/2002GL015783, 2002. 12221
Rex, M., von der Gathen, P., Harris, N. R. P., Lucic, D., Knudsen, B. M., Braathen, G. O., Reid, S. J., De Backer, H., Claude, H., Fabian, R., Fast, H., Gil, M., Kyrö, E., Mikkelsen, I. S., Rummukainen, M., Smit, H. G., Stähelin, J., Varotsos, C., and Zaitcev, I.: In situ Measurements of stratospheric ozone depletion rates in the Arctic winter 1991/92: A Lagrangian approach, J. Geophys. Res., 103, 5843–5853, 1998. 12241
Schoeberl, M. R. and Newman, P. A.: A multiple-level trajectory analysis of vortex filaments, J. Geophys. Res., 100, 25 801–25 815, 1995. 12241
Schumann, U., Huntrieser, H., Schlager, H., Höller, H., Bugliaro, L., and Gatzen, C.: Results from experiments over Europe and the continental tropics, in Proceedings DACH-Meteorologentagung, Karlsruhe, 1–10, 2004. 12234
Sherwood, S. C. and Dessler, A. E.: A model for transport across the tropical tropopause, J. Atmos. Sci., 58, 765–779, 2001. 12219
Simmons, A. J., Untch, A., Jakob, C., Kållberg, P., and Unden, P.: Stratospheric water vapour and tropical tropopause temperatures in ECMWF analyses and multi-year simulations, Q. J. R. Meteorol. Soc., 125, 353–386, 1999. 12225, 12226
Smagorinsky, J.: General circulation experiments with the primitive equations: I. The basic experiment, Mon. Wea. Rev., 91, 99–164, 1963. 12242
Stefanutti, L., McKenzie, A. R., Santacesaria, V., Adriani, A., Balestri, S., Borrmann, S., Khattatov, V., Mazzinghi, P., Mitev, V., Rudakov, V., Schiller, C., Toci, G., Volk, C. M., Yushkov, V., Flentje, H., Kiemle, C., Redaelli, G., Carslaw, K. S., Noone, K., and Peter, T.: The APE-THESEO Tropical Campaign: An Overview, J. Atmos. Chem., 48, 1–33, 2004. 12230
Stohl, A.: A one-year Langrangian "climatology" of airstreams in the northern hemisphere troposphere and lowermost stratosphere, J. Geophys. Res., 106, 7263–7280, 2000. 12241
Tie, X., Zhang, R., Brasseur, G., Emmons, L., and Lei, W.: Effects of lightning on reactive nitrogen and nitrogen reservoir species in the troposphere, J. Geophys. Res., 106, 3167–3178, 2001. 12235
Tie, X., Brasseur, G., and Lei, W.: Global NOx production by lightning, J. Atmos. Chem., 43, 61–74, 2002. 12235
Tiedtke, M.: A comprehensive mass flux scheme for cumulus parameterization in large-scale models, Mon. Wea. Rev., 117, 1779–1800, 1989. 12226, 12242
Voigt, C., Schlager, H., Luo, B., Dörnbrack, A., Roiger, A., Stock, P., Curtius, J., Vössing, H., Borrmann, S., Davies, S., Konopka, P., Schiller, C., Shur, G., and Peter, T.: Nitric acid

trihydrate (NAT) formation at low NAT supersaturations, Atmos. Chem. Phys., 5, 1371–1380, 2004. 12230

Wernli, H. and Davies, H. C.: A Lagrangian-based analysis of extratropical cyclones I: The method and some applications, Q. J. R. Meteorol. Soc., 123, 467–489, 1997. 12235

Zhong, W. and Haigh, J. D.: Improved Broadband Emissivity Parameterization for Water Vapor Cooling Rate Calculations, J. Atmos. Sci., 52, 124–138, 1995. 12225

Zhou, J. and Lau, K. M.: Does a Monsoon Climate Exist over South America?, J. Climate, 11, 1020–1040, 1998. 12230

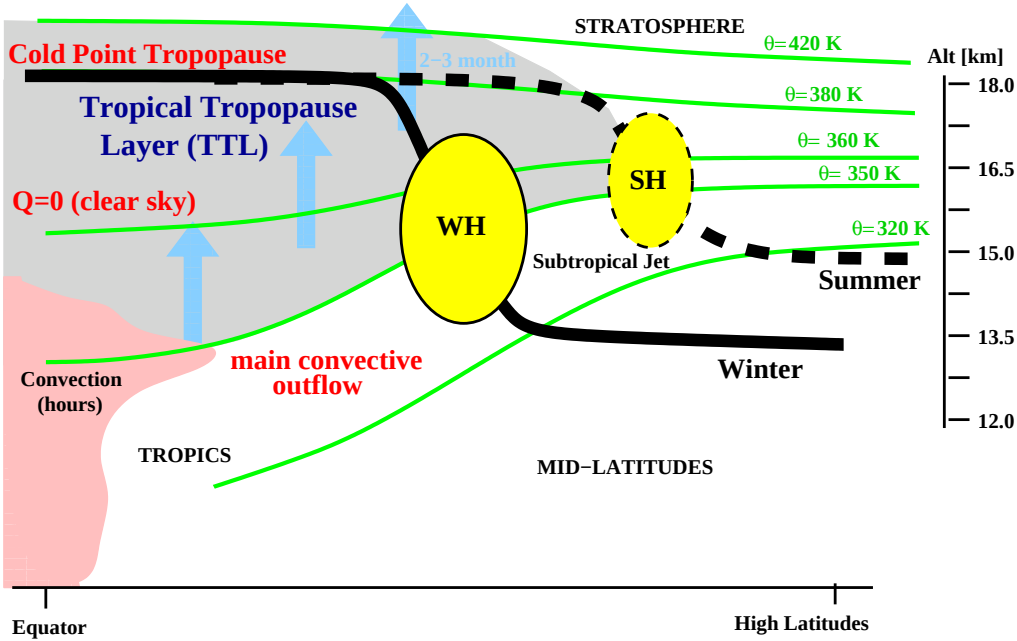

Fig. 1. Schematic of the troposphere-to-stratosphere transport (TST) occurring in the TTL. This transport path starts approximately at the main convective outflow level around 350 K and, following the blue arrows, crosses the level of zero clear sky radiative heating (Q=0) around 360 K, and finally, reaches the lower stratosphere above the cold point tropopause around 380 K.

ACPD
6, 12217–12266, 2006

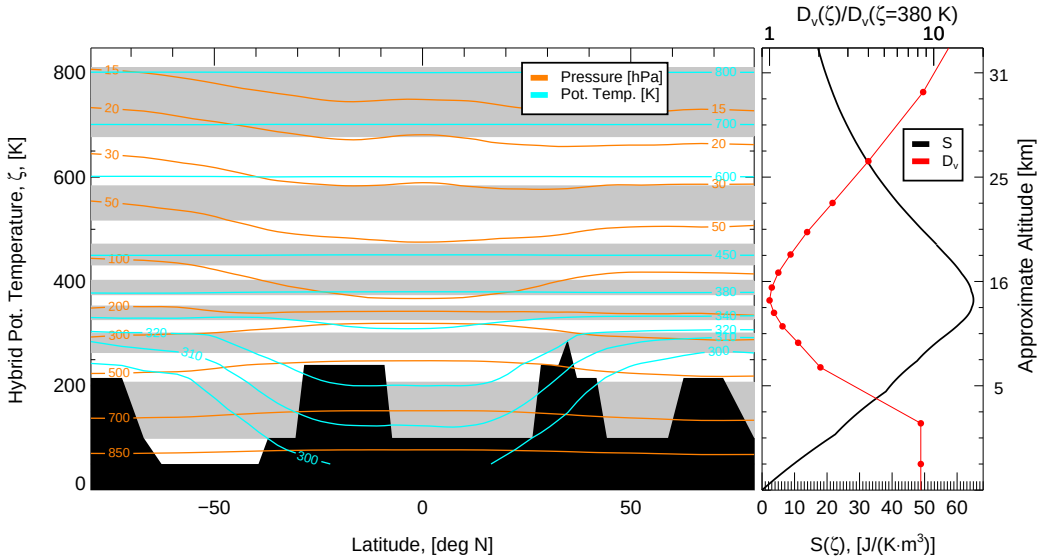

Fig. 2. CLaMS hybrid vertical coordinate ζ. Left: Entropy preserving CLaMS layers $\Delta\zeta$ colored alternating with gray and white are overlaid with the isolines of zonally averaged pressure p (black) and potential temperature θ (orange) (for illustration derived for one ECMWF data set at 1 January 2004, 12:00 UT). Right: Entropy density profile $S(\zeta)$ (black) derived from equation (3) for the U.S. standard atmosphere. The condition ΔS=const in every layer $\Delta\zeta$ was used to generate CLaMS layers. The red bold dots denote the relative vertical diffusivity $D_v(\zeta)/D_v(\zeta{=}380\,\mathrm{K})$ calculated for one mixing event between two adjacent AP.

ACPD
6, 12217–12266, 2006

EGU

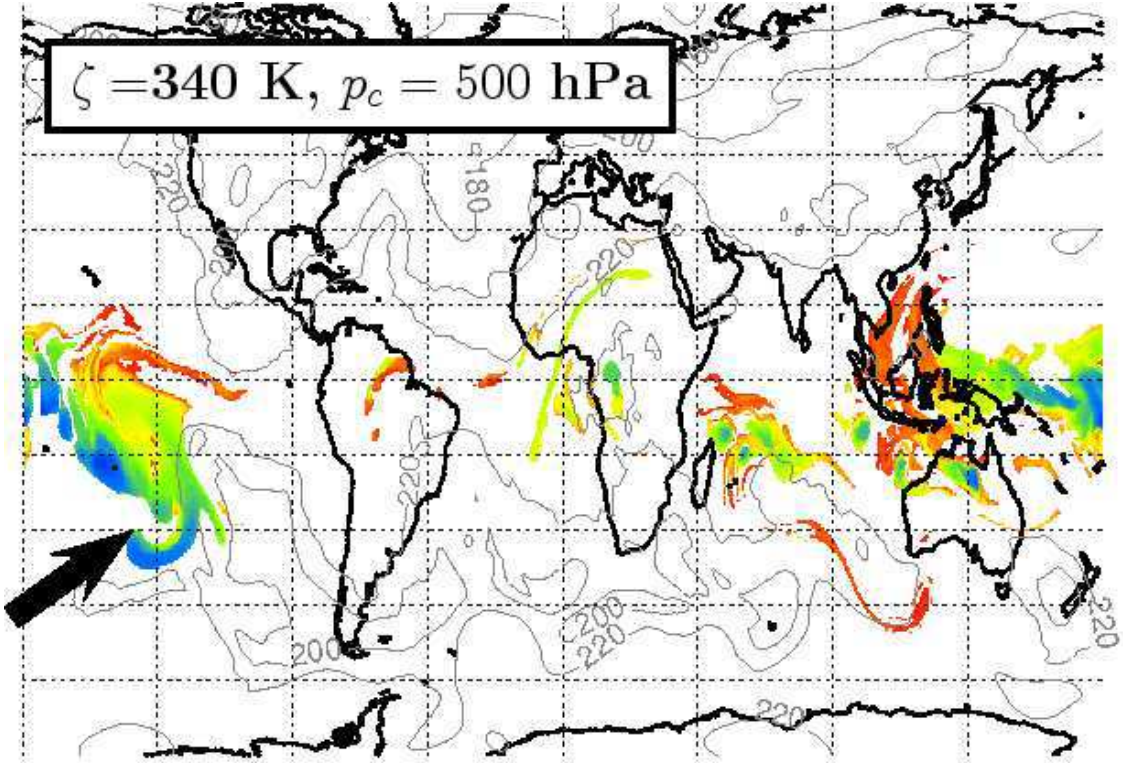

Fig. 3a. Age of convection (top and middle panel) and the ECMWF water vapor distribution at ζ=340 K (bottom). The age of convection is derived from the backward trajectories starting at this level on 8 Febrauary 2005, 12:00 UT and is defined as the time lag between the initialization time and the time when the trajectory descended below p_c=500 (top) and p_c=300 hPa (middle). The gray-colored lines denote the pressure isolines.

ACPD
6, 12217–12266, 2006

EGU

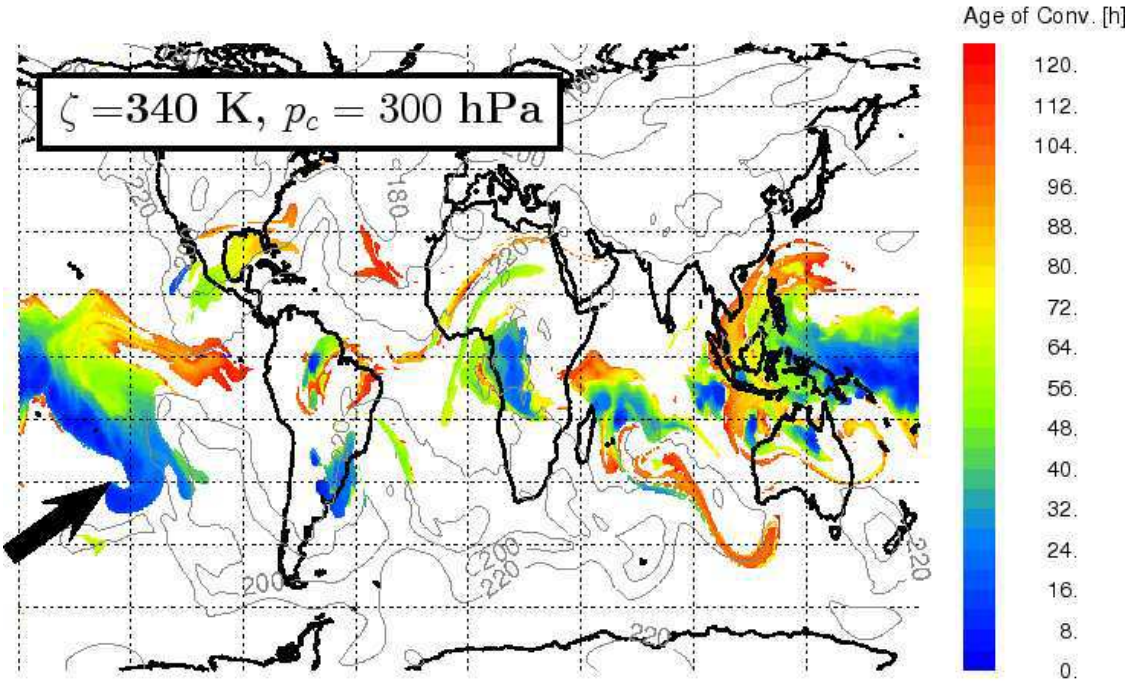

Fig. 3b. Age of convection (top and middle panel) and the ECMWF water vapor distribution at ζ=340 K (bottom). The age of convection is derived from the backward trajectories starting at this level on 8 Febrauary 2005, 12:00 UT and is defined as the time lag between the initialization time and the time when the trajectory descended below p_c=500 (top) and p_c=300 hPa (middle). The gray-colored lines denote the pressure isolines.

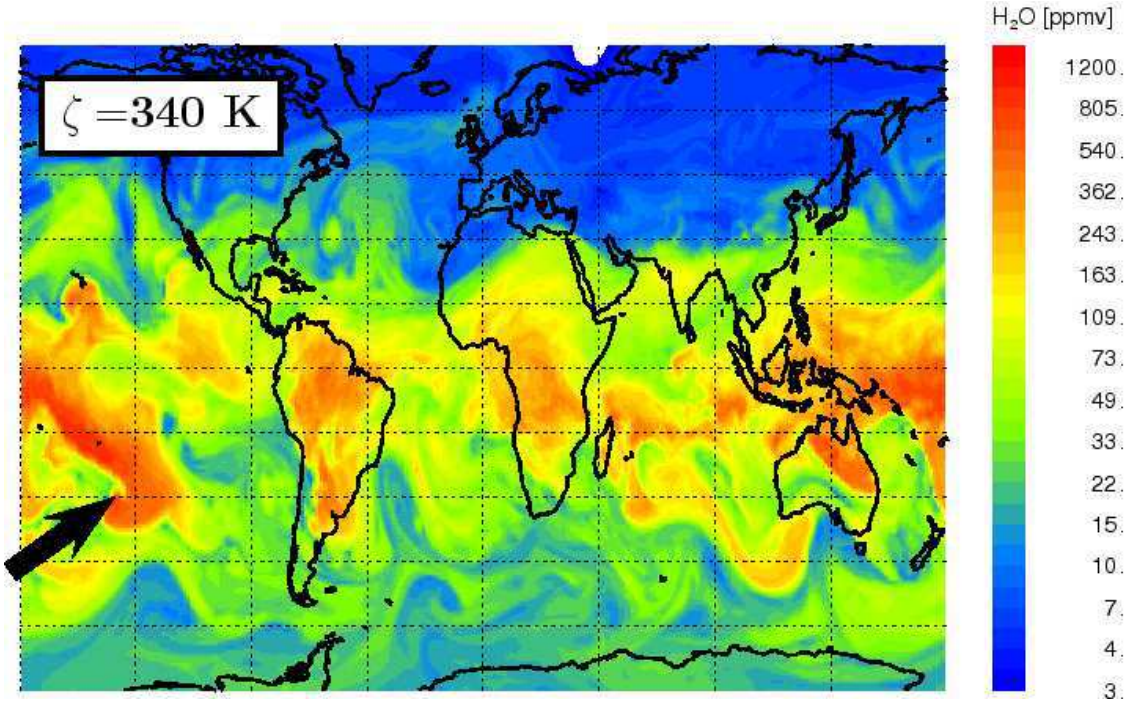

Fig. 3c. Age of convection (top and middle panel) and the ECMWF water vapor distribution at ζ=340 K (bottom). The age of convection is derived from the backward trajectories starting at this level on 8 Febrauary 2005, 12:00 UT and is defined as the time lag between the initialization time and the time when the trajectory descended below p_c=500 (top) and p_c=300 hPa (middle). The gray-colored lines denote the pressure isolines.

ACPD
6, 12217–12266, 2006

EGU

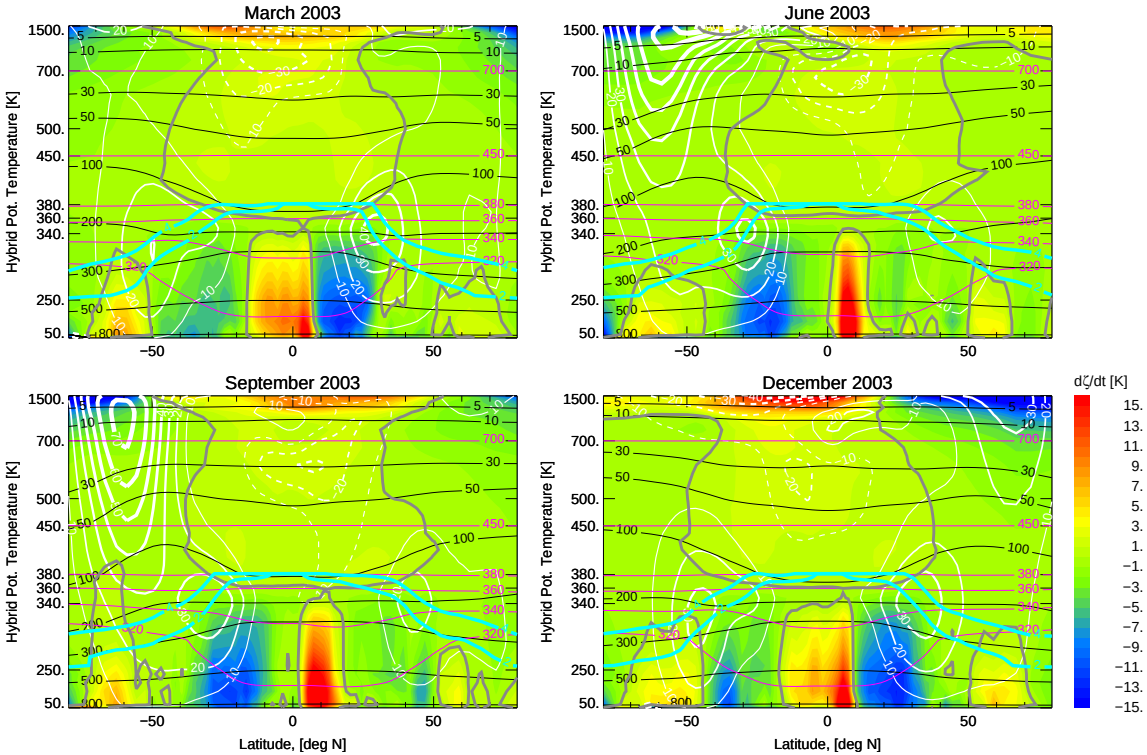

Fig. 4. Zonally and monthly averaged vertical velocities $\dot{\zeta}$ shown as the function of the entropy-weighted hybrid coordinate θ (i.e. the entropy density along the vertical axis is constant). The gray contour defined by $\dot{\zeta}$=0 separates the ascent from descent regions. White contours (solid – westerlies, dashed – easterlies) describe the zonal wind. The isolines of pressure (black) and potential temperature (pink) are overlaid. The isolines |PV|=2 and 4 PVU together with the θ=380 K line (blue) approximate the position of the tropopause in the extra-tropics and in the tropics, respectively.

ACPD
6, 12217–12266, 2006

Contribution of mixing to the upward transport across the TTL

P. Konopka et al.

EGU

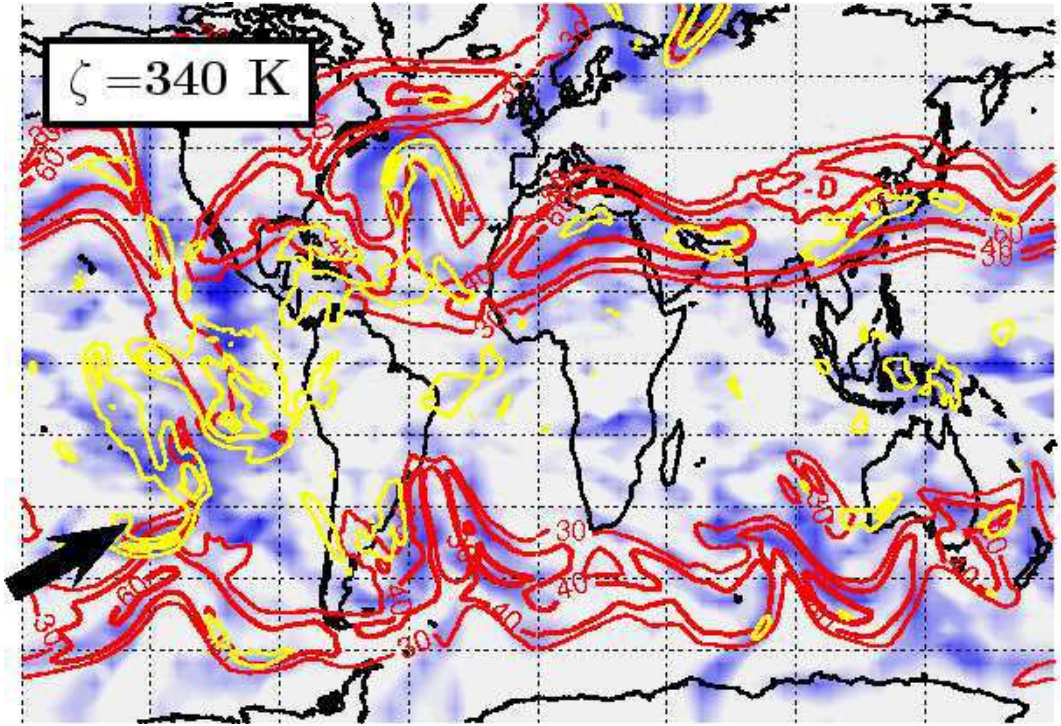

Fig. 5a. CLaMS vertical diffusivity D_v on 8 February 2005 at ζ=340, 360 and 380 K from top to bottom as implemented in CLaMS by the deformation-induced mixing procedure (blue shaded). Overlaid are contours of the absolute horizontal wind velocity u (red) plotted for 30, 40, and 60 m/s with increasing thickness together with the contours of the absolute vertical shear of the horizontal wind $|du/d\zeta|$ (yellow) shown for 0.4, 0.7, and 0.9 m/sK. Whereas high values of u estimate the position of the subtropical jets, the enhanced values of $|du/d\zeta|$ can be found either near the jets, preferably above the jet core, or in the tropics. The latter are located, to some extend, in the outflow of fresh convection (black arrows, compare for with Fig. 7).

ACPD
6, 12217–12266, 2006

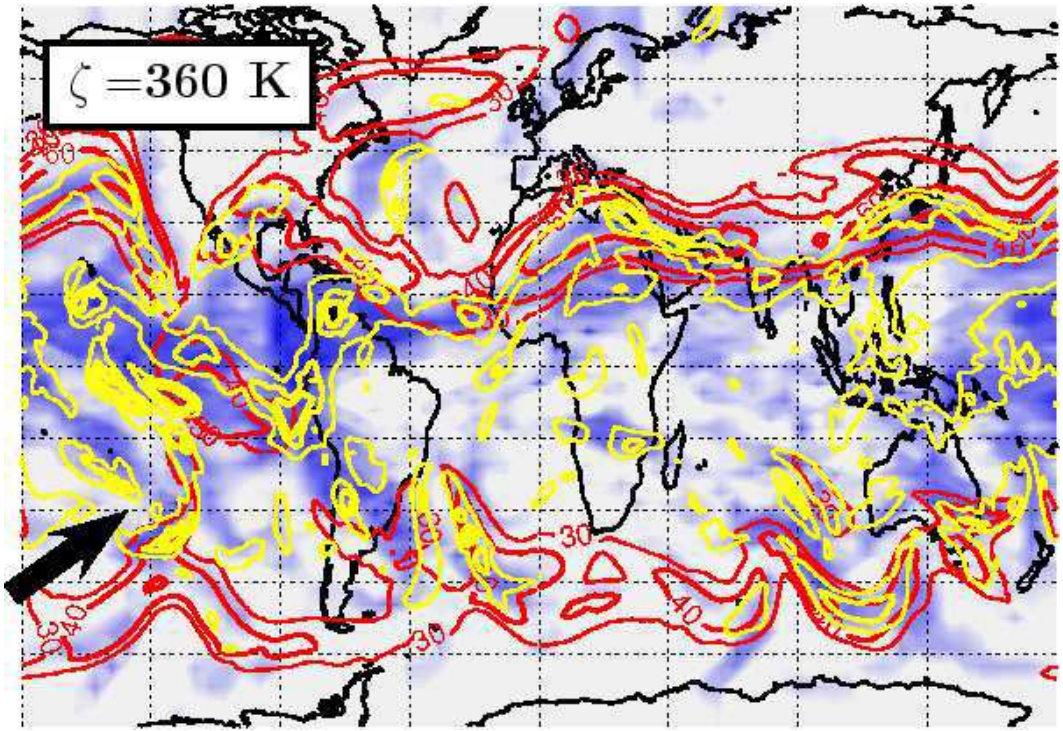

Fig. 5b. CLaMS vertical diffusivity D_v on 8 February 2005 at ζ=340, 360 and 380 K from top to bottom as implemented in CLaMS by the deformation-induced mixing procedure (blue shaded). Overlaid are contours of the absolute horizontal wind velocity u (red) plotted for 30, 40, and 60 m/s with increasing thickness together with the contours of the absolute vertical shear of the horizontal wind $|du/d\zeta|$ (yellow) shown for 0.4, 0.7, and 0.9 m/sK. Whereas high values of u estimate the position of the subtropical jets, the enhanced values of $|du/d\zeta|$ can be found either near the jets, preferably above the jet core, or in the tropics. The latter are located, to some extend, in the outflow of fresh convection (black arrows, compare for with Fig. 7).

ACPD
6, 12217–12266, 2006

EGU

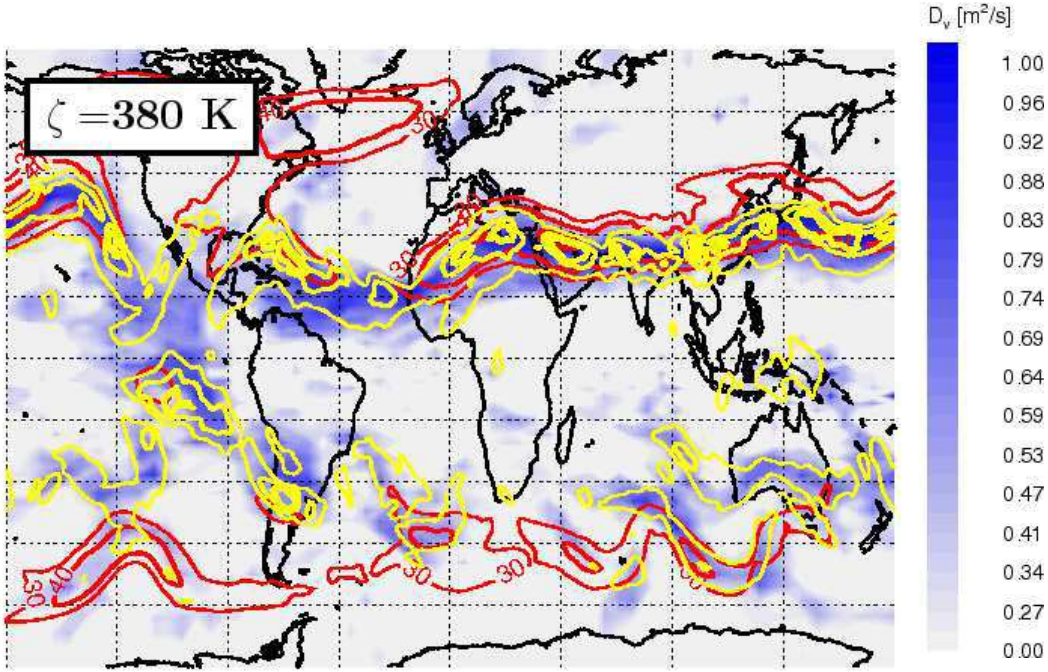

Fig. 5c. CLaMS vertical diffusivity D_v on 8 February 2005 at ζ=340, 360 and 380 K from top to bottom as implemented in CLaMS by the deformation-induced mixing procedure (blue shaded). Overlaid are contours of the absolute horizontal wind velocity u (red) plotted for 30, 40, and 60 m/s with increasing thickness together with the contours of the absolute vertical shear of the horizontal wind $|du/d\zeta|$ (yellow) shown for 0.4, 0.7, and 0.9 m/sK. Whereas high values of u estimate the position of the subtropical jets, the enhanced values of $|du/d\zeta|$ can be found either near the jets, preferably above the jet core, or in the tropics. The latter are located, to some extend, in the outflow of fresh convection (black arrows, compare for with Fig. 7).

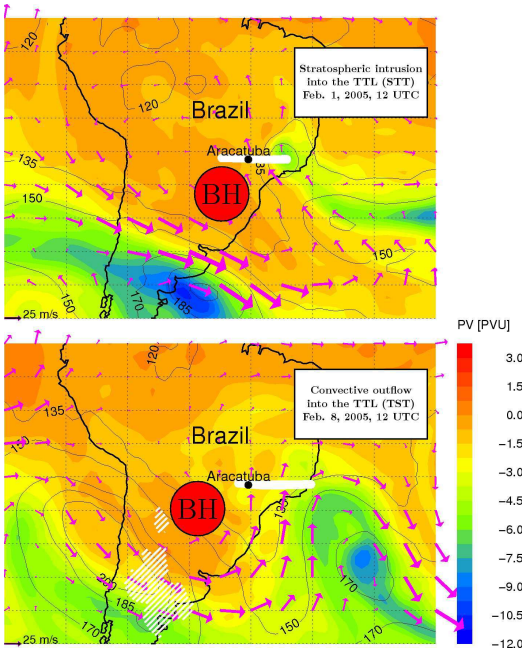

Fig. 6. Map of ECMWF potential vorticity (PV) at θ=360 K on 1 February (top) and on 8 February, 12:00 UT (bottom). On these 2 days signatures of STE were observed (white thick lines denote the flight tracks). Pink arrows show the horizontal wind with highest values in the STJ surrounding the upper-level, quasi-stationary Bolivian high (BH). The black lines are pressure isolines (in hPa). Top: Air masses with low PV values (blue) east of Araçatuba are trapped in the TTL by a cut-off low. These air masses have been separated from the lowermost stratosphere, transported along the STJ and mixed into the TTL (STT). Bottom: MCS over Argentina and South Brazil (white dashed contours denote regions with ECMWF-H_2O >25 ppmv on 7 February, 06:00 UT, i.e about 32 h prior the flight) transports air masses from the boundary layer up to about 330–340 K. Vertical mixing along the STJ lifts these air masses up to about 360 K, where cirrus clouds, enhanced water vapor, and increased NO/NO_y ratios were observed (TST).

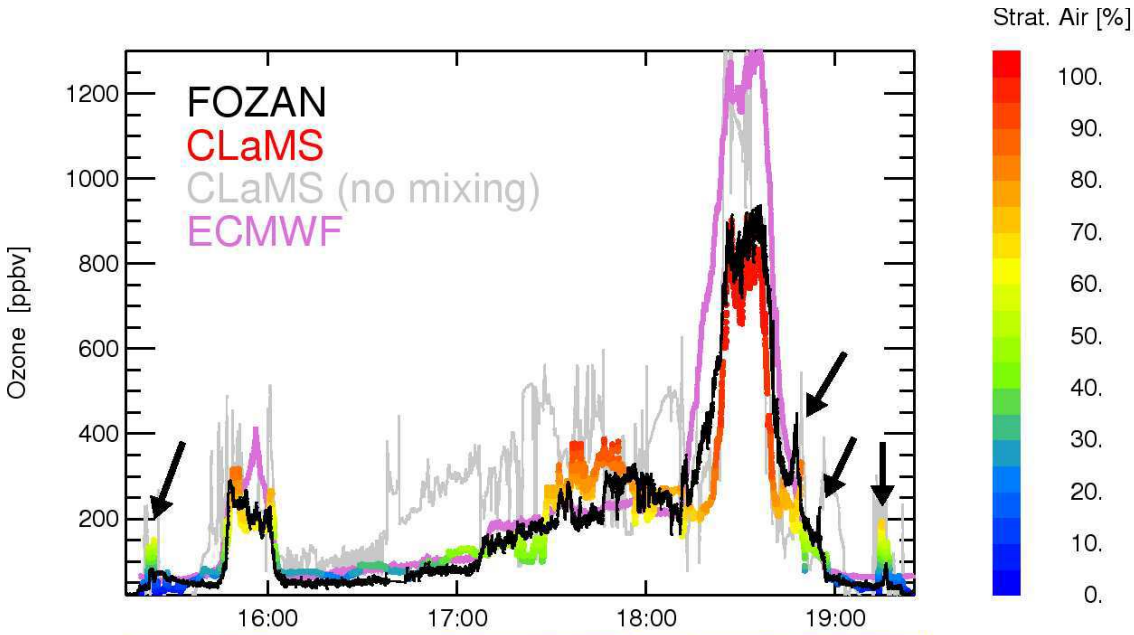

Fig. 7a. Top: Ozone observations (FOZAN-black, ECMWF-pink) and CLaMS simulations colored with the percentage of the stratospheric tracer ST (Strat. Air) within the observed air masses as modeled by CLaMS during the flight on 1 February. Bottom left: The vertical distribution of CLaMS ST tracer along the flight track. Thin black and pink lines are p and θ-isolines, respectively. The tropopause defined as |PV| = 2 PVU surface (violet), the Q=0 level (dark gray) and the isotachs (light gray) indicating the position of the STJ are also shown. Bottom right: FOZAN profiles as observed during all local flights (gray) compared with the profile measured on 1 February and colored with the ST tracer.

ACPD
6, 12217–12266, 2006

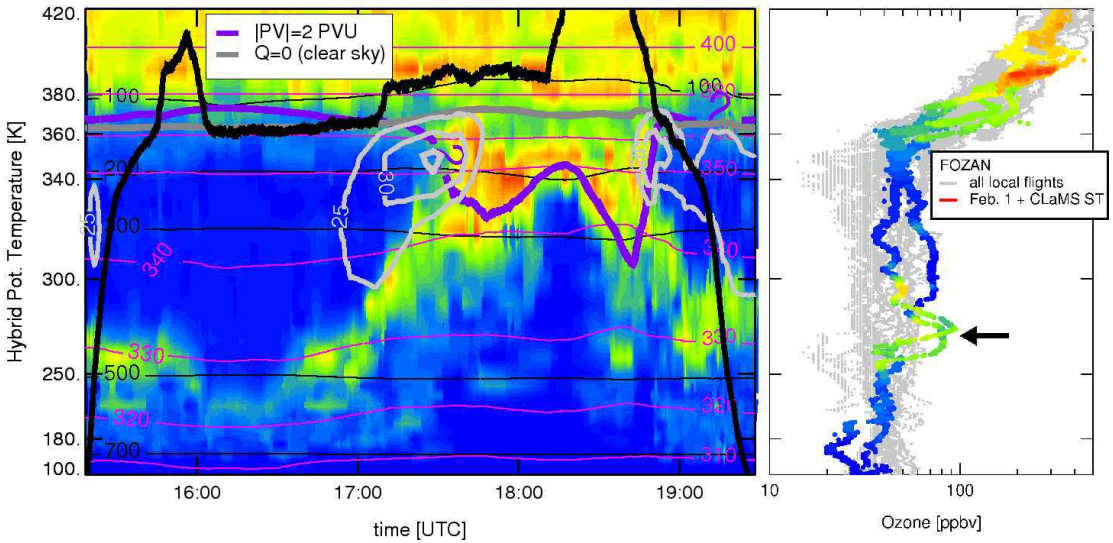

Fig. 7b. Top: Ozone observations (FOZAN-black, ECMWF-pink) and CLaMS simulations colored with the percentage of the stratospheric tracer ST (Strat. Air) within the observed air masses as modeled by CLaMS during the flight on 1 February. Bottom left: The vertical distribution of CLaMS ST tracer along the flight track. Thin black and pink lines are p and θ-isolines, respectively. The tropopause defined as |PV| = 2 PVU surface (violet), the Q=0 level (dark gray) and the isotachs (light gray) indicating the position of the STJ are also shown. Bottom right: FOZAN profiles as observed during all local flights (gray) compared with the profile measured on 1 February and colored with the ST tracer.

ACPD
6, 12217–12266, 2006

EGU

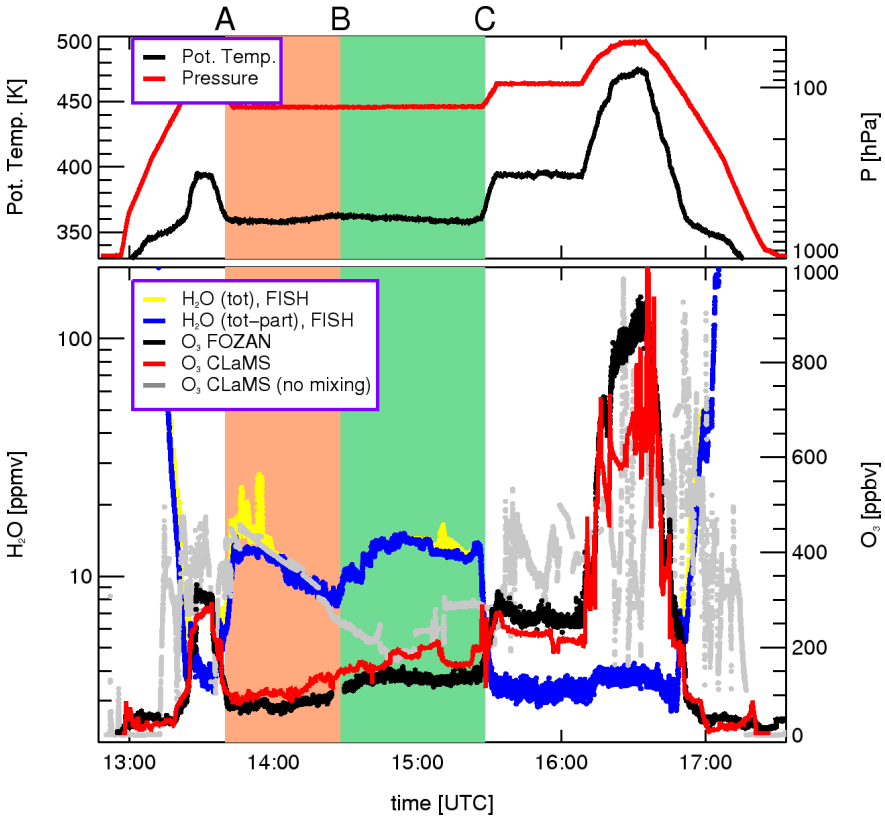

Fig. 8. Flight on 8 February. Top: Potential temperature (black) and pressure (red) along the flight track. Bottom left: Total water (yellow) and water vapor (blue) as observed by FISH instrument. Bottom right: Observed (black) and simulated ozone with (red) and without mixing (gray). In the beige (AB) and green (BC) colored segments of the flight (≈360 K), pure tropospheric and mixed, i.e. tropospheric and stratospheric signatures were observed which, using CLaMS, can be explained as a consequence of mixing within the TTL.

ACPD
6, 12217–12266, 2006

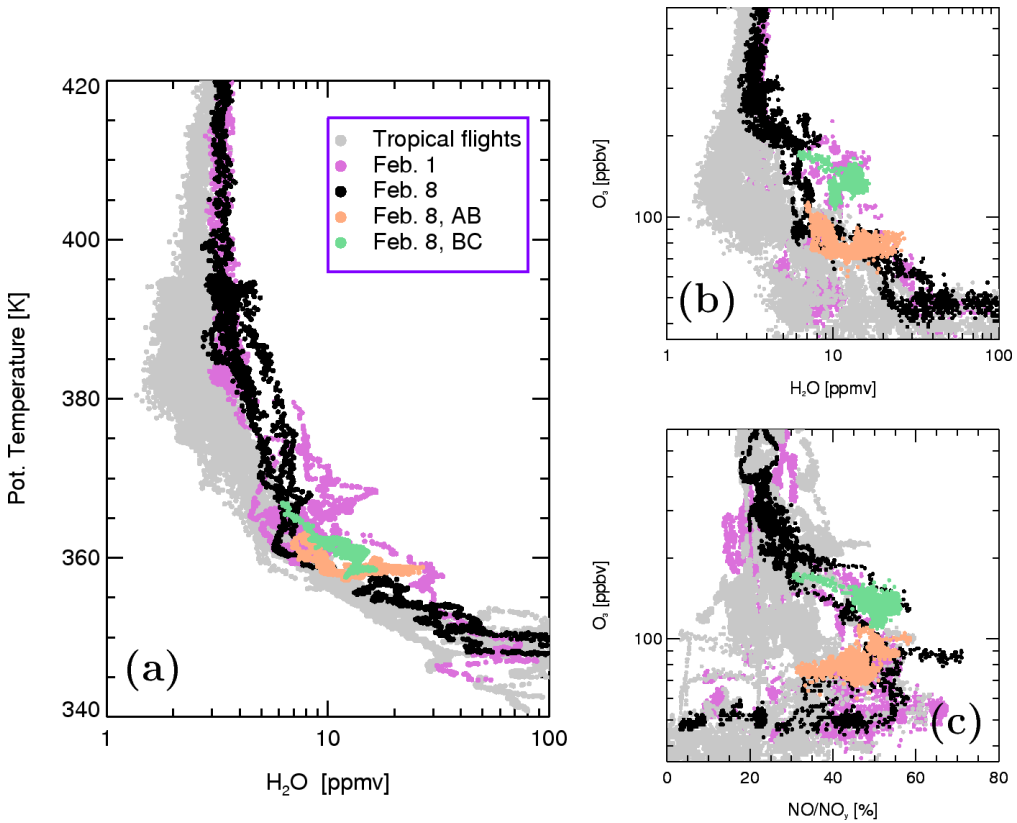

Fig. 9. Profiles of total water **(a)**, correlations of ozone with total water **(b)** and NO/NO_y **(c)** during the flight on 8 February (black) and 1 February (violet) compared with pure tropical flights (gray). The contributions from the AB and BC flight segments are colored beige and green, respectively.

ACPD
6, 12217–12266, 2006

EGU

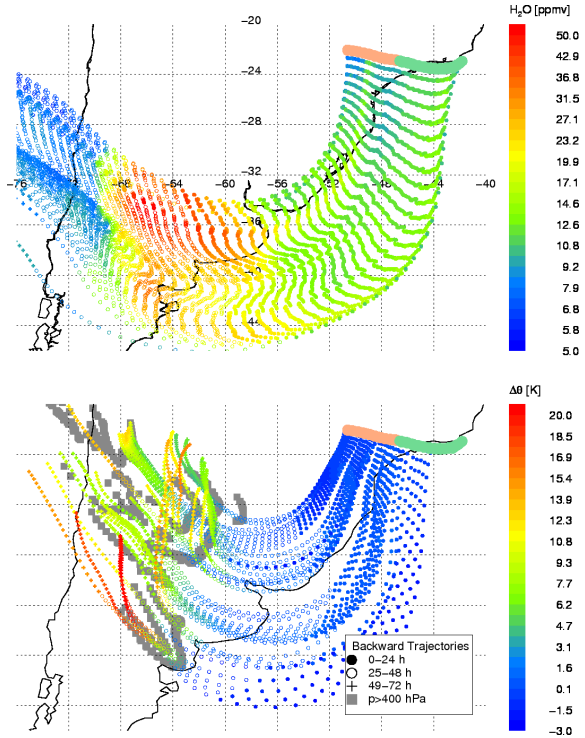

Fig. 10. 3-days backward trajectories starting on 8 February 2005 between 13:45 and 15:30 UT from the AB (beige) and BC (green) flight legs (top) or 25 K below these flight legs (bottom). Top: ECMWF H_2O interpolated along these trajectories. Bottom: $\Delta\theta$ experienced by the air masses along the backward trajectories starting 25 K below the flight track. Positive (red) and negative (blue) values correspond to up- and downward motion of air with increasing time. The gray footprints are places where the trajectories crossed the 400 hPa level. In the satellite pictures (GOES), fresh convective clouds could be found in the same region (see Fig. 11).

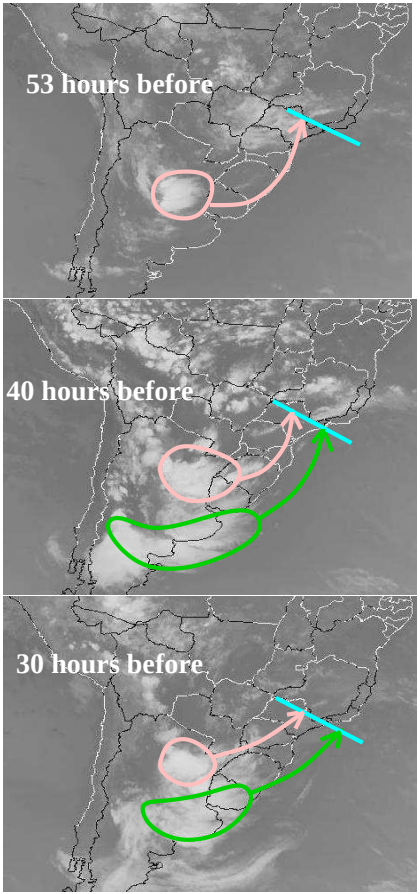

Fig. 11. Convection as detected by the GEOS satellite 53 (top), 40 (middle) and 30 h (bottom) prior the flight on 8 February.

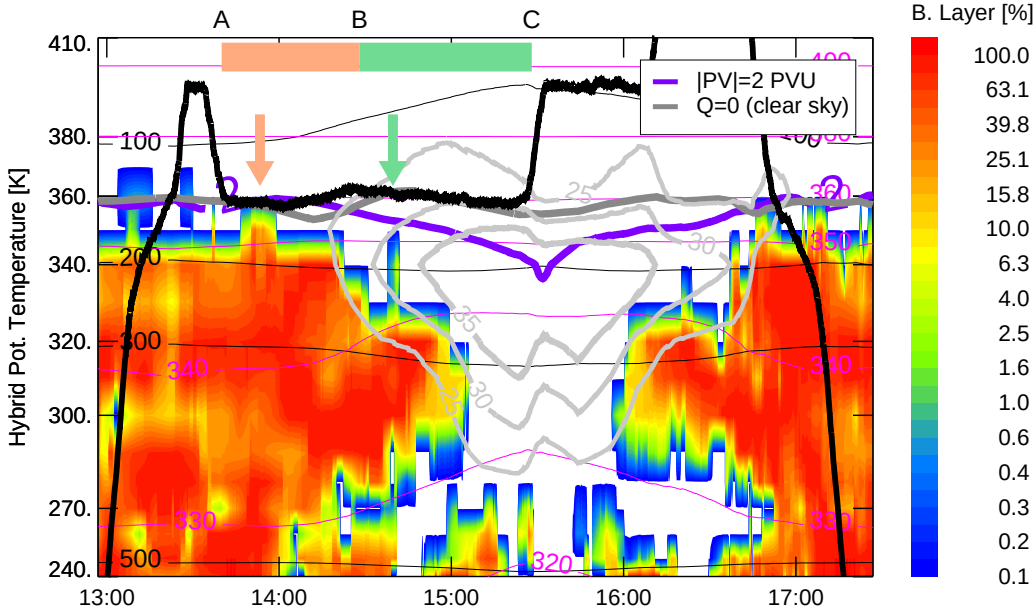

Fig. 12. Vertical distribution of the BL tracer (B. Layer) along the flight track on 8 February 2005. Here, BL was re-initialized 3 days before the flight to 100% and 0 above and below 400 hPa, respectively. The distribution of this tracer shows that mixing has the potential to lift the air masses from the convective outflow around θ=335 K up to 360 K (white means no BL contribution in this region). The tropopause (|PV|=2 PVU, violet), the Q=0 level (dark gray) and the isotachs (light gray) indicating the position of the STJ are also shown.

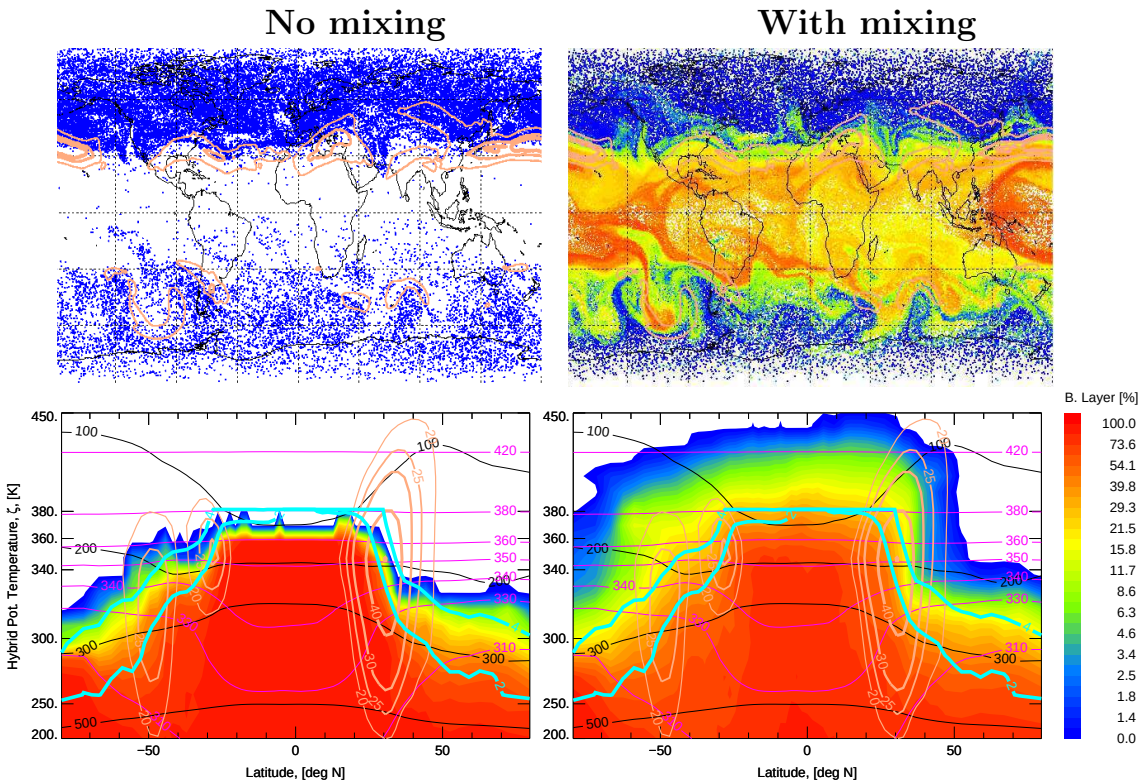

Fig. 13. Horizontal distribution of CLaMS BL tracer (B. Layer) at ζ=380 K (top row) and zonally averaged vertical distribution of BL (bottom row) after more than 3 months of transport (108 days) on 7 March 2005 calculated without (left) an with (right) mixing.

ACPD
6, 12217–12266, 2006

EGU

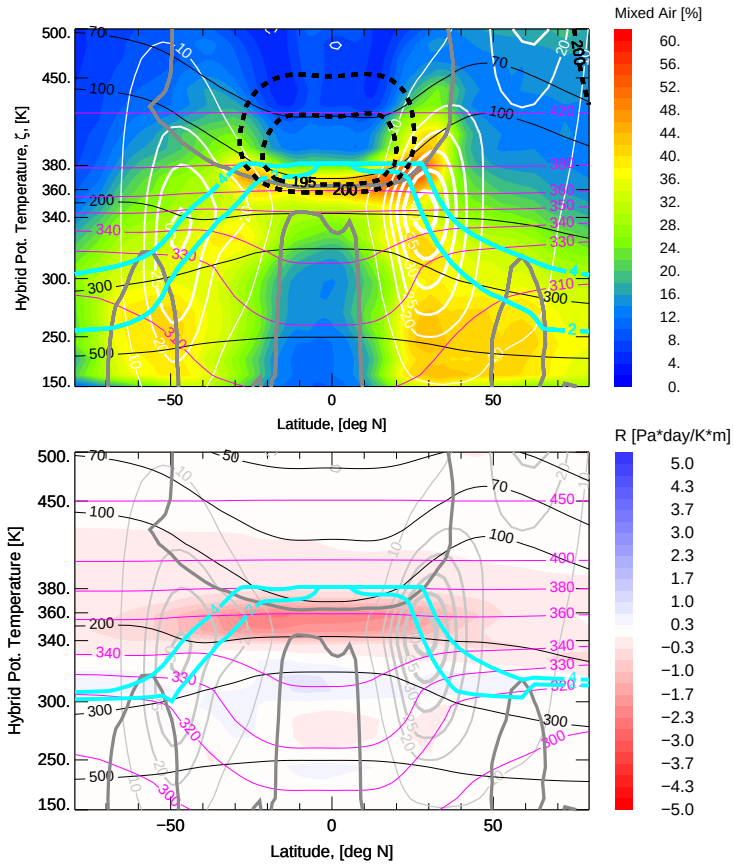

Fig. 14. Mean mixing intensity plotted as the percentage of AP affected by mixing (top) and the mean residual of the continuity equation R calculated in ζ-coordinates (bottom) and zonally averaged over the entire simulation time (108 days). The isotachs of the wind (light gray), Q=0 line, and the blue lines approximating the tropopause.

ACPD
6, 12217–12266, 2006

Contribution of mixing to the upward transport across the TTL

P. Konopka et al.

EGU